Competitive Influence Maximization in Voter Dynamics: The Role of Timing and Network Heterogeneity

Zhongqi Cai^{a,b,*}, Enrico Gerding^b and Markus Brede^b

^aSchool of Computer and Information Engineering, Xiamen University of Technology, Xiamen, China

ARTICLE INFO

Keywords: Influence maximization Voter model Complex networks Opinion dynamics

ABSTRACT

In the study of influence maximization, most existing research often assumes a one-off resource allocation at the start of a competition. As a result, they overlook the benefits of dynamic, time-sensitive strategies. To overcome this limitation, we propose a novel approach using intertemporal allocations within a non-progressive voter model to optimize the timing and distribution of limited resources for maximizing opinion spread. Our objective is twofold: (i) to provide understanding of patterns of opinion spread in complex networks subject to inter-temporal control, and (ii) to use insights from (i) to develop optimization strategies that balance resource constraints and temporal dynamics. Specifically, our study examines two scenarios: a constantopponent setting and a game-theoretical framework. In the constant-opponent setting, we find that network heterogeneity significantly influences optimal campaign timing, with late initiation benefiting short time horizons in heterogeneous networks and early starts favoring longer horizons. To further enhance this strategy, we introduce a node-specific optimization strategy that outperforms uniform approaches, especially under resource constraints. In the game-theoretical framework, our results reveal that resource-rich controllers tend to start campaigns early, while resource-limited controllers strategically delay to counter their opponent's advantage. Through analytical approximations and simulations, we provide insights into the temporal dynamics of influence spread. These findings offer practical guidelines for designing effective influence campaigns in competitive and time-sensitive contexts, with applications in marketing, politics, and public health.

1. Introduction

The intervention from influential agents in social networks can yield substantial social and commercial impacts, particularly evident in scenarios like viral marketing [24, 48], political campaigns [5, 18], and significant societal movements such as the Brexit campaign [46] or general radicalization [22]. Understanding how these influential agents shape public discourse is crucial for mitigating manipulative practices or steering public opinion constructively. Central to this is the concept of influence maximization (IM) [28], where influential agents, acting as external controllers, strategically deploy resources (e.g., money, information, incentives) to maximize their influence within the network. This approach typically operates within a budget constraint, as resources available for allocations to agents are often inherently limited [6, 28].

Existing IM research has predominantly relied on progressive models, such as the independent cascade (IC) and linear threshold (LT) models [11, 13, 24]. These models assume that once individuals adopt an opinion, they maintain it indefinitely. While these models have yielded valuable insights into influence dynamics [50], they fail to capture the bi-directional and reversible opinion shifts common in real-world scenarios. For instance, studies have demonstrated that opinions often fluctuate and oscillate over time due to various mechanisms, such as aging effects [45] and response latency [44]. These opinion fluctuations, also common in political campaigns, public health messaging, and social movements, reflect how individuals continuously update their views through social interactions and in response to new information.

Recognizing the limitations of progressive models, researchers have increasingly turned to non-progressive models [35, 39, 42] that account for multiple state changes and reversible influence. Among these, we choose the voter model in this study, which allows opinions to change iteratively through neighbor interactions, reflecting how people adapt their views based on ongoing social influence. This choice is motivated by three key factors beyond the prominence of

^bSchool of Electronics and Computer Science, University of Southampton, Southampton, UK

^{*}Corresponding author

[🕯] zhongqicai@xmut.edu.cn (Z. Cai); eg@ecs.soton.ac.uk (E. Gerding); Markus.Brede@soton.ac.uk (M. Brede)

the voter model in research [49]. First, its conceptual simplicity provides analytical tractability, which enables detailed analysis of how network structure shapes opinion propagation or consensus formation [39]. Second, the model captures the evolution of opinions towards minimal conflict states, which realistically represents opinion formation or consensus processes [14]. Third, the voter model aligns with empirical observations, such as election outcomes in the USA and UK [9, 19, 54], demonstrating its practical relevance.

In addition to the limitations posed by the prevalent use of progressive influence models, another significant gap in current IM research lies in the focus on maximizing opinion spreads at equilibrium – the state after dynamics stabilize [33]. This approach, while valuable for understanding long-term outcomes, often fails to capture the critical transient dynamics that precede equilibrium. However, in many real-world scenarios, such as seasonal promotions, political campaigns, and public health interventions, the ability to influence opinions swiftly and effectively is crucial for achieving impact [26]. For instance, during a flu outbreak, rapidly disseminating vaccination information and encouraging uptake within a short time frame is crucial to preventing widespread infection, while a political campaign must shape public opinion before election day. These scenarios highlight the need to develop strategies that optimize influence during transient phases and better understand the spread of opinions in networks under temporal control.

Regarding this, recent studies have begun to integrate temporal considerations into IM [1–3, 10, 23, 34, 53]. However, most of existing approaches fail to allow time-variant resource allocations or focus exclusively on single-controller scenarios, which limits their relevance to competitive, real-world contexts. For instance, the most directly relevant work to our modeling approach is by Brede et al. [10], who first explored time-constrained influence maximization in the voter model. While their work provides valuable insights into the impact of time constraints on IM strategies, it does not allow for varying resource allocations over time. This limitation restricts its ability to capture real-world flexibility in dynamically optimizing budgets to respond to the evolving landscape of opinions and market conditions. Beyond Brede et al. [10], several studies have explored the timing of influence strategies [1–3, 53]. Specifically, Alshamsi et al. [3] focus on speeding up diffusion by strategically targeting individuals with varying connectivity levels at different stages of diffusion. Tong et al. [53] advance this concept by adapting strategies in response to early outcomes of diffusion. However, a common limitation in these studies is their focus on scenarios with only a single influencer (controller). This simplification restricts their applicability in real-world competitive contexts like politics or radicalization prevention [47, 55], where multiple influencers interact and compete for influence.

The only studies solving inter-temporal influence maximization in the competitive setting are [1] and [2], which utilize reinforcement learning for node selection and timing. However, their frameworks are built on progressive models, which assume monotonic opinion shifts and are unable to capture real-world scenarios where opinions fluctuate based on events, new information, or peer interactions. Furthermore, to manage computational complexity, they rely on predefined, discrete seed selection and timing strategies, which limits their ability to develop robust optimization strategies for complex networks under inter-temporal control. Additionally, they do not investigate the interplay between timing strategies and transient opinion dynamics, leaving unexplored how network structure shapes opinion spread patterns under inter-temporal control.

To address these research gaps in the inter-temporal IM problem, our paper leverages transient dynamics to maximize influence within both time and budget constraints based on the non-progressive voter model. Specifically, our study has two primary objectives: (i) to develop optimization strategies that balance resource constraints and temporal dynamics by identifying the optimal timing of resource deployment to steer opinion trajectories effectively over short timescales, and (ii) to decode the black-box nature of numerical optimization outcomes by analyzing how these intertemporal control strategies shape opinion dynamics across different network structures. A key aspect of this approach involves navigating a critical trade-off in resource allocations: Delaying resource allocations might offer more budget per time unit but reduces the time window for influence to manifest. Conversely, earlier allocations allow more time for the impact to accumulate. However, this can lead to inefficiency as resources might be wasted before the critical period when the impact of the allocations is finally measured. Through systematic analysis of this temporal trade-off, our study aims to provide both theoretical insights and optimization strategies under transient control in complex networks.

Our exploration of the inter-temporal IM is structured into two main scenarios: the constant-opponent setting and the game-theoretical setting. In the constant-opponent setting, we analyze the dynamics of an active controller competing against an opponent with a predetermined, unchanging strategy. We first investigate a simplified model where the active controller only decides the starting point of its campaign, applying resources uniformly across all individuals in the network. We then extend this to more sophisticated numerical simulations involving individual optimization and agent heterogeneity. This progression allows us to isolate the effects of timing and resource distribution, providing insights into the fundamental dynamics of influence spread. Moreover, in the game-theoretical

setting, we introduce strategic competition between two controllers, where both strive to maximize their influence without prior knowledge of their opponent's strategy. This scenario more closely mimics real-world competitive environments, where multiple actors simultaneously attempt to shape public opinion. By examining the strategies that emerge in this setting, we gain insights into the complex interplay between timing, resource allocation, and competitive dynamics in influence maximization.

By doing so, we make the following contributions. (i) Building upon our previous work [12], we provide the first comprehensive study of IM from the perspective of inter-temporal allocations using non-progressive models. This approach marks a significant shift from traditional static allocation methods, which enables a more accurate representation of the dynamic nature of influence spread in social networks. (ii) By employing the heterogeneous mean-field method [10] and utilizing Taylor expansions, we derive analytical approximations that provide insights into the temporal dynamics of influence spread. These techniques enable us to quantify the timescales required for networks to reach equilibrium, with a particular focus on scale-free networks. Moreover, this analytical framework enhances the understanding of the patterns and outcomes of inter-temporal strategies. (iii) Our framework derives optimal strategies in both constant-opponent and game-theoretical settings. In constant-opponent scenarios, we newly incorporate agent heterogeneity to reflect realistic variations in susceptibility. We also extend our investigation to include game-theoretical scenarios under uniform strategies, a novel aspect not explored in [12]. (iv) Through extensive numerical experiments, we demonstrate that inter-temporal optimized influence strategies consistently outperform baseline approaches. This highlights the importance of optimizing both timing and resource allocation to adapt to the dynamic and competitive nature of influence propagation. Our findings also provide actionable guidelines for practitioners in various domains, such as targeted marketing, public health interventions, and social media campaigns with insights into designing effective, time-sensitive influence strategies.

We obtain the following main findings: (i) In the constant-opponent scenario, the best strategy for the active controller is to delay its influence. This involves initially allowing the system to be dominated by the opponent, and then strategically deploying its budget towards the campaign's end. Notably, for shorter timeframes, the active controller tends to begin its influence relatively later in networks with high heterogeneity than in more homogeneous ones. Conversely, for longer time horizons, initiating control earlier is advantageous in highly heterogeneous networks. (ii) In the game-theoretical context, the controller with a larger budget typically commences its influence earlier than its opponent. This preemptive start aims to secure a lead in vote shares before its rival begins its influencing efforts. (iii) Compared to the simplified scenario where all agents begin at the same time, individual optimization shows a relatively modest advantage when total budgets are equal or more than that of the opponent. In contrast, in settings where the active controller has fewer resources, individual optimization, focusing on influencing agents with fewer connections, can significantly improve the final vote shares. (iv) Regarding agent heterogeneity within the individual optimization scenario, we observe that agents that are less susceptible to influence (for example, staunch supporters) are prioritized with more resources and should be targeted earlier when the active controller has a substantial budget. Conversely, with a smaller budget, these agents are deprioritized.

The structure of this paper is as follows: Section 2 introduces the formulation and algorithms for inter-temporal IM, covering constant-opponent, node-specific, and game-theoretical settings. Section 3 presents the heterogeneous mean-field analysis, which provides theoretical approximations for understanding opinion dynamics under temporal control. Section 4 provides experimental results, including the dataset setup, network heterogeneity impact, and analysis of optimal strategies across constant-opponent, individual optimization, and game-theoretical settings. Finally, Section 5 summarizes the findings and outlines future research directions.

2. Formulation and Algorithms for Inter-temporal Allocations

In this study, we conceptualize social networks through the mathematical framework of graphs denoted as G(V, E). Here, vertices $v_i \in V$ for $i = 1, \dots, N$ represent a collection of N individuals, and edges $w_{ij} \in E$ denote the magnitude of interactions between individuals i and j. Adhering to prevalent conventions in network studies, our model assumes un-directed graphs with positive edge weights and excludes self-loops. In our model, agents can hold one of two distinct opinions: A or B. In addition to these internal agents, the model incorporates two external entities, referred to as controller A and controller A, supporting opinion A or A, respectively. Unlike the internal agents in the network, these two controllers maintain their opinions unchanged at all time, and exert influence on agents in the network without being affected in return. To influence the network, controllers can strategically build time-varying, unidirectional links with agents in the network. The strength of the influence at time t is captured by control gains $a_i(t)$ and $b_i(t)$ for

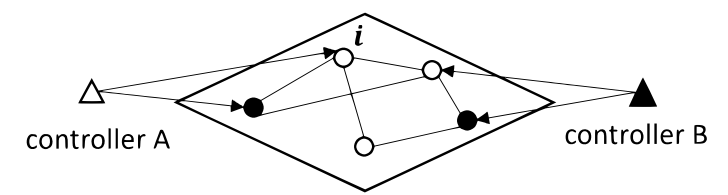


Figure 1: Schematic diagram of how controllers interact with the opinion dynamics and how agents update their opinions. Triangles stand for controllers and agents are represented by circles. White and black symbols indicate that the agents (or controllers) are holding opinions A or B, respectively. The lines between agents correspond to the social connections. External controllers A and B influence opinion dynamics by building unidirectional links to agents in the networks. Assuming unit link weights from the neighbours and controllers, if picked for updating, agent i will have probability 3/4 to stay in opinion A and probability 1/4 to flip its opinion.

controllers A and B, respectively. These gains reflect how much resource is allocated to agent i at time t and the sum of these gains is subject to the budget constraints: $\sum_{i} \int a_{i}(t)dt \le b_{A}$ for controller A and $\sum_{i} \int b_{i}(t)dt \le b_{B}$ for controller B, where b_A and b_B are the total resources for each controller. Moreover, control gains must be non-negative, i.e., $a_i(t) \ge 0$ and $b_i(t) \ge 0$.

The opinion updating process with competing controllers using the voter model is described as follows [39]. At each time step t, an agent i is randomly selected from the network. Then, agent i chooses to interact with either a neighboring agent or one of the controllers. The choice is weighted, with probabilities tied to the strength of the connection, including any influence exerted by the controllers given by the control gains $a_i(t)$ or $b_i(t)$. More specifically, the likelihood of agent i adopting a particular opinion is determined as follows. (i) For adopting the opinion of a network neighbour, the probability is $\frac{w_{ji}}{\sum_{\ell=1}^{N} w_{\ell i} + a_i(t) + b_i(t)}$. (ii) For adopting the opinion of controller A, the probability is $\frac{a_i(t)}{\sum_{\ell=1}^{N} w_{\ell i} + a_i(t) + b_i(t)}$. (iii) For adopting the opinion of controller B, the probability is $\frac{b_i(t)}{\sum_{\ell=1}^{N} w_{\ell i} + a_i(t) + b_i(t)}$.

is
$$\frac{a_i(t)}{\sum_{\ell=1}^N w_{\ell i} + a_i(t) + b_i(t)}$$
. (iii) For adopting the opinion of controller B , the probability is $\frac{b_i(t)}{\sum_{\ell=1}^N w_{\ell i} + a_i(t) + b_i(t)}$.

For a better understanding of the opinion updating process, consider a real-world scenario illustrated in Fig. 1. Imagine a social media user, Alice (represented as agent i), who is deciding whether to support a new city policy (opinion A) or oppose it (opinion B). In Fig. 1, Alice is connected to three friends on the social network. Two friends (represented by white circles) support the policy (opinion A), while one friend (represented by a black circle) opposes the policy (opinion B). Additionally, Alice sees a sponsored post from a group advocating for the policy (controller A, represented by a white triangle). When Alice logs onto the platform and starts scrolling through her feed (analogous to being "picked" for updating in our model), she's exposed to these various opinions. Assuming all connections (friend relationships and the sponsored post) have equal influence strength, Alice's opinion update process works as follows: The probability of Alice maintaining support for the policy (staying with opinion A) is 3/4. This comes from the two supporting friends plus one sponsored post, out of four total influences. Conversely, the probability of Alice changing to oppose the policy (flipping to opinion B) is 1/4, stemming from the one opposing friend, out of four total influences. Therefore, while Alice is more likely to continue supporting the policy due to the majority influence, there's still a chance she might change her mind based on her opposing friend's influence.

Here, following the work by Masuda [39], we employ the mean-field rate equation for describing probability flows. Specifically, we introduce $x_i(t)$ as the probability that agent i adopts opinion A at time t. Consequently, the dynamic of $x_i(t)$ is determined by the following differential equation:

$$\frac{dx_i(t)}{dt} = \left(1 - x_i(t)\right) \frac{\sum_j w_{ji} x_j(t) + a_i(t)}{\sum_j w_{ji} + a_i(t) + b_i(t)} - x_i(t) \frac{\sum_j \left(1 - x_j(t)\right) w_{ji} + b_i(t)}{\sum_j w_{ji} + a_i(t) + b_i(t)}.$$
 (1)

In Eq.(1), the first term quantifies the transition of agents from holding opinion B to adopting opinion A, influenced by their peers and external control. The second term, in contrast, tracks the shift from opinion A to B, considering similar effects.

Building on this framework, the goal of controller A is to maximize its influence in the network, quantified as the vote share at time T:

$$S_A(T) = \frac{1}{N} \sum_{N} x_i(T). \tag{2}$$

Here, $S_A(T)$ denotes the fraction of agents holding opinion A across the whole network at time T.

Note that, the system dynamics described by Eq. (1) are non-autonomous, driven by the time-dependent control variables $a_i(t)$ and $b_i(t)$. Fully flexible influence allocation using these continuous variables is both computationally and theoretically infeasible for large networks due to the high dimensionality of the solution space and the interdependence among agents. Even in the simplified single-node case analyzed in Appendix A, deriving solutions requires resolving a transcendental equation. As the network size increases, the problem's complexity grows exponentially, exacerbated by the intricate coupling between agent states and control variables. These difficulties underscore the need for simplified models and computational approximations. To this end, we develop our analysis through three progressive stages of increasing complexity. We begin with a simplified model in Section 2.1 that focuses solely on determining the optimal starting time for one of the controller, rather than considering arbitrary control functions. This approach, while simplified, provides valuable insights into vote share trajectories and opinion control strategies. We then advance to a more sophisticated model in Section 2.2 that incorporates agent-specific allocations and start times. This refinement enables more complicated influence strategies while preserving computational tractability. Finally, we examine the game-theoretical framework in Section 2.3 where both controllers actively compete against each other.

2.1. Inter-temporal Allocations against a Constant Opponent

We first examine the scenario where controller A competes against a constant opponent influence. In this setting, we optimize a uniform campaign strategy characterized by a single start time and equal resource allocation across all agents. Our objective remains maximizing the vote share for opinion A at time T, as defined in Eq. (2), while competing against controller B who maintains a constant influence from the beginning of the competition. This formulation allows us to isolate the temporal aspects of campaign optimization before introducing more complex strategic interactions. Specifically, the influence of controllers A and B on each agent i (where $1 \le i \le N$) can be expressed as:

$$a_i(t) = \begin{cases} 0 & 0 \le t \le t_a \\ \frac{b_A}{(T - t_a)N} & t_a < t \le T, \end{cases}$$

$$b_i(t) = \frac{b_B}{TN} \qquad 0 \le t \le T,$$

$$(3)$$

where t_a represents the controller A's campaign start time for all agents.

To elucidate this scenario, consider the following example based on a social media influence campaign: Let G(V, E) represent a social network with $|V| = N = 10^4$ users. The competition duration T is set to 30 days, representing a month-long campaign. Initially, 55% of users favor opinion $A(S_A(0) = 0.55)$ and 45% favor opinion $B(S_B(0) = 0.45)$. Controllers A and B have advertising budgets of $b_A = 1.5 \times 10^4$ and $b_B = 1.2 \times 10^4$ respectively. Under these conditions, the influence functions from Eq. (3) become:

$$a_{i}(t) = \begin{cases} 0 & 0 \le t \le t_{a} \\ \frac{1.5 \times 10^{4}}{(30 - t_{a})10^{4}} & t_{a} < t \le 30, \end{cases}$$

$$b_{i}(t) = \frac{1.2 \times 10^{4}}{30 \times 10^{4}} = 0.04 \qquad 0 \le t \le 30,$$

$$(4)$$

Here, $a_i(t)$ and $b_i(t)$ can be interpreted as the daily advertising spend per user (in dollars) for controllers A and B respectively. This formulation illustrates the trade-off controller A faces in determining t_a . For instance: If A starts immediately ($t_a = 0$), it spends 0.05 per user per day over 30 days. If A delays by 15 days ($t_a = 15$), it spends 0.10 per user per day, but only for the latter 15 days. Meanwhile, B maintains a constant spend of 0.04 per user per day throughout the 30-day period.

The inter-temporal influence maximization problem thus reduces to identifying the optimal start time t_a^* that maximizes $S_A(T)$.

$$t_a^* = \underset{t_a}{\arg\max} S_A(T) \quad \text{for} \quad 0 \le t_a \le T.$$
 (5)

Here, $S_A(T)$ is the fraction of agents holding opinion A at time T defined in Eq. (2). We solve this optimization problem using the interior-point algorithm [4]. The choice of the interior-point method is driven by its robustness and efficiency in handling large-scale, constrained optimization problems, which are typical in influence maximization scenarios.

2.2. Inter-temporal Allocations with Individual Optimization

Above, we have investigated the inter-temporal allocations in a simplified scenario. As it may be too restrictive to assume that all nodes start at the same time with the same intensity, a question naturally arises: if the controller has more flexibility to deploy its resources, will it lead to a significant improvement in obtainable vote share? Regarding this, we have proposed the individual optimization scenario where the controller can choose different starting times and split its resources unevenly over individual nodes. Specifically, we consider a case in which controller A can choose specific campaigning starts $t_{a,i}$ for individual node i and has the option to split its budget unevenly between nodes by assigning individual node i with budget $b_{A,i}$. To reduce the number of parameters we still retain the assumption that, once started, campaigns proceed with constant intensity, i.e.,

$$a_{i}(t) = \begin{cases} 0 & 0 \le t \le t_{a,i} \\ \frac{b_{A,i}}{(T - t_{a,i})} & t_{a,i} < t \le T \end{cases}$$
 (6)

where $b_{A,i}$ should satisfy $\sum_i b_{A,i} = b_A$.

Correspondingly, the optimization problem expands to incorporate both temporal and resource allocation decisions across individual agents. In other words, we need to optimize two variables for each agent i: the campaign start time $t_{A,i}$ and the budget allocation $b_{A,i}$. The optimization problem can be formally expressed as:

$$\max_{t_{a,i},b_{A,i}} S_A(T) \quad \text{ for } \quad \sum_i b_{A,i} = b_A, \, b_{A,i} \ge 0, \quad 0 \le t_{a,i} \le T \tag{7}$$

where $S_A(T)$ is the vote shares at time T. Here, we use the stochastic hill climbing algorithm for the individual optimization. The pseudo-code for the algorithm is presented in Algorithm 1, and its detailed procedure is described below: (i) Start with a given network configuration and an initialization of starting times $\{0 \le t_{a,i} <= T\}$ and budget allocations $\{b_{A,i}\}$ for each agent $i=1,\cdots,N$. Note that, the initial budget allocations $\{b_{A,i}\}$ should meet the budget constraint $\sum_i b_{A,i} = b_A$. In practice, we set the initial budget allocations as $\{b_{A,i}\} = b_A/N$. Let L_{max} be the maximum number of iterations. Then, compute the vote share of the initial configuration via Eqs. (1) and (2) (see lines 1-2 in Algorithm 1). (ii) If the current iteration is less than L_{max} , continue with step (iii). Otherwise, jump to step (iv) (line 4). (iii) Generate a random number r according to the uniform distribution with lower bound 0 and upper bound 1 (line 5). If r < 0.5, randomly pick two nodes i and j ($i \ne j$), and transfer a random fraction of budget allocations from node i to node j (lines 6-15). It's important to note that transferring budgets between nodes ensures the total budget remains unchanged, thus satisfying the budget constraint. Otherwise, randomly select one node and randomly modify its starting time within the range of [0,T] (lines 17-23). Update the vote share only if improvements are achieved via the above modification. Return to step (ii). (iv) The procedure is ended (line 27).

2.2.1. Individual Optimization Considering Agent Heterogeneity

Building on the individualized optimization framework, we next incorporate agent heterogeneity to better reflect real-world network dynamics. Following established research on voter models [40, 41], we introduce the concept of partial zealots agents with inherent biases towards particular opinions. Specifically, we introduce a zealotry parameter, q_i , representing the probability that node i, when holding opinion B, resists adopting opinion A despite neighbor or controller influence. Consequently, the rate equation for the probability, x_i , of agent i holding opinion A becomes:

$$\frac{dx_{i}(t)}{dt} = (1 - q_{i}) \left(1 - x_{i}(t) \right) \frac{\sum_{j} w_{ji} x_{j}(t) + a_{i}(t)}{\sum_{j} w_{ji} + a_{i}(t) + b_{i}(t)} - x_{i}(t) \frac{\sum_{j} \left(1 - x_{j}(t) \right) w_{ji} + b_{i}(t)}{\sum_{j} w_{ji} + a_{i}(t) + b_{i}(t)} \\
= \left(1 - q_{i} + q_{i} x_{i}(t) \right) \frac{a_{i} + \sum_{j} w_{ij} x_{j}(t)}{k_{i} + a_{i} + b_{i}} - x_{i}(t). \tag{8}$$

Note that, our probabilistic approach to modeling opinion persistence described in Eq. (8) differs fundamentally from latency-based mechanisms like [30], where agents enter waiting periods of complete resistance after an opinion change. While latency models provide insights into how temporary opinion freezing affects system-wide opinion propagation, partial zealotry instead captures continuous variations in resistance levels. This distinction allows us to explore how heterogeneous susceptibility patterns influence strategic resource allocation and campaign outcomes.

Additionally, this enhanced model captures several key aspects of real-world influence campaigns. First, it acknowledges that individuals have varying susceptibilities to persuasion, reflecting natural differences in opinion

```
input: b_A, N, T, maximum iterations L_{max}, adjacency matrix A
    output: Optimal starting times \{t_{a,i}\}, optimal budget allocations \{b_{A,i}\}, maximized vote share S_A^{best}
 1 Initialize: t_{a,i} = random \ values \ in [0,T]; \ b_{A,i} = b_A/N \ for \ all \ i;
    S_A^{best} = compute \ vote \ share \ using \ Eqs. (1) \ and (2);
 3 iteration = 0;
 4 while iteration < L_{max} do
          r = \text{random number from uniform distribution } [0,1];
 6
          if r < 0.5 then
                randomly select nodes i, j \ (i \neq j);
 7
                \delta = random fraction of b_{A,i};
 8
                \begin{split} b_{A,i}^{temp} &= b_{A,i} - \delta; \\ b_{A,j}^{temp} &= b_{A,j} + \delta; \end{split}
 9
10
                S_A^{new} = \text{compute vote share with } \{b_{Ai}^{temp}\};
11
                if S_A^{new} > S_A^{best} then
\begin{vmatrix} b_{A,i} = b_{A,i}^{lemp}; b_{A,j} = b_{A,j}^{temp}; \\ S_A^{best} = S_A^{new}; \end{vmatrix}
12
13
14
                end
15
          else
16
                randomly select node i;
17
                t_{a,i}^{temp} = random value in [0,T];
18
                S_A^{new} = compute vote share with t_{ai}^{temp};
19
                if S_A^{new} > S_A^{best} then
\begin{vmatrix} t_{a,i} = t_{a,i}^{lemp}; \\ S_A^{best} = S_A^{new}; \end{vmatrix}
20
21
22
23
          end
24
          iteration = iteration + 1;
25
26 end
27 return \{t_{a,i}\}, \{b_{A,i}\}, S_A^{best}
```

Algorithm 1: Stochastic Hill Climbing for Individual Optimization

formation processes. Second, it allows us to study how these inherent biases interact with strategic resource allocation decisions. Third, it provides insights into the role of network structure when agents exhibit heterogeneous behavior. Similarly, in this scenario, the optimization involves two variables for each agent i: the campaign start time $t_{a,i}$ and the budget allocation $b_{A,i}$ as described in Eq. (7) with $a_i(t)$ and $b_i(t)$ defined in Eq. (6). To achieve this, we employ the stochastic hill climbing algorithm outlined in Algorithm 1 with dynamics defined in Eq. (8).

2.3. Inter-temporal Allocations in the Game-theoretical Setting

In Section 2.1, we investigate the competitive influence maximization for one of the competing controllers. In this section we explore the game-theoretic aspects of competitive influence allocations. Specifically, in the game-theoretical scenario, we consider a zero-sum game of competitive vote-share maximization on social networks. Players of the game are controller A and controller B who have complete knowledge of graph G. In addition, the two players have to simultaneously decide on an inter-temporal allocation protocol at time zero. In the simplified campaign scheme, both controllers have the flexibility to choose the starting time of allocations, defined as t_a and t_b . More precisely, the sets of actions available to controller A and controller B are $\phi_A = \{t_a \mid 0 \le t_a \le T\}$ and $\phi_B = \{t_b \mid 0 \le t_b \le T\}$ respectively.

Hence, agent i's $(1 \le i \le N)$ budget allocation per unit time is given by:

$$a_{i}(t) = \begin{cases} 0 & 0 \le t \le t_{a} \\ \frac{b_{A}}{(T - t_{a})N} & t_{a} < t \le T \end{cases}$$

$$b_{i}(t) = \begin{cases} 0 & 0 \le t \le t_{b} \\ \frac{b_{B}}{(T - t_{b})N} & t_{b} < t \le T \end{cases}$$

$$(9)$$

Moreover, the payoff functions for controller A and B are $u_A = S_A(T)$ and $u_B = 1 - S_A(T)$ where the vote shares $S_A(T)$ are continuous and satisfy $0 \le S_A(T) \le 1$.

While pure-strategy Nash equilibria are theoretically guaranteed to exist in two-player zero-sum games under continuity, convexity and boundedness assumptions [37], explicitly calculating these equilibria through analytical means remains challenging for games with infinite, continuous strategy spaces [25]. This holds in our problem setting, where the unknown strategies used by the opponent yield continuous action spaces that are mathematically intractable for closed-form equilibrium analysis. Additionally, the absence of closed-form expressions for the payoff functions of either competing controller further hinders direct analytical tractability for deriving equilibria. Given these constraints, we develop an iterative numerical approach to approximate the Nash equilibria based on the minimax theorem [20]. This approach builds on the work of Bonomi et al. [8] but adapts their framework to the specific context of inter-temporal influence maximization in the voter model. More specifically, this algorithm operates on the minimax theorem's key insight: in a two-player zero-sum game, each player can achieve their optimal strategy by maximizing their objective function while accounting for their opponent's minimization efforts. We implement this through iterative maximization and minimization of $S_A(T)$, with several important modifications for our context. First, we introduce an adaptive learning rate μ ($0 \le \mu \le 1$) [36] that decreases with each iteration. This adaptation helps ensure stable convergence by gradually reducing step sizes as the algorithm progresses toward equilibrium. Additionally, we develop specific initialization and update rules for the starting times t_a and t_b that reflect the unique constraints of our intertemporal allocation framework. The complete algorithm implementation is detailed in Algorithm 2.

```
input: b_A, b_B, N, T, adjacency matrix A, threshold \theta output: approximations for t_a^{NE} and t_b^{NE} at Nash equilibria; corresponding vote shares at time T, S_A(T) 1 Initialization: t_a^{(0)} = 0; t_b^{(0)} = 0; \Delta t_a = 1; \Delta t_b = 1; i = 0; 2 while \left| \Delta t_a \right| + \left| \Delta t_b \right| \ge \theta do 3 \left| t_a^{(i+1)} = t_a^{(i)} + \mu \left( \arg \max_{t_a} \left\{ S_A(T) \middle| t_b = t_b^{(i)} \right\} - t_a^{(i)} \right); 4 \left| t_b^{(i+1)} = t_b^{(i)} + \mu \left( \arg \min_{t_b} \left\{ S_A(T) \middle| t_a = t_a^{(i+1)} \right\} - t_b^{(i)} \right); 5 \left| \Delta t_a = t_a^{(i+1)} - t_a^{(i)} \right|; 6 \left| \Delta t_b = t_b^{(i+1)} - t_b^{(i)} \right|; 7 \left| i = i + 1 \right|; 8 \left| \mu = 1/i \right|; 9 end 10 t_a^{NE} = t_a^{(i-1)}; 11 t_b^{NE} = t_b^{(i-1)}; 12 S_A(T) = \{S_A(T) \mid t_a = t_a^{NE}, t_b = t_b^{NE} \}
```

Algorithm 2: Iterative searching for Nash equilibria

Algorithm 2 begins by initializing the start times of controllers A and B ($t_a^{(0)}$ and $t_b^{(0)}$) to zero, indicating that both controllers initially begin their influence strategies at the earliest possible time (see line 1). The step sizes Δt_a and Δt_b are initially set to 1, and the iteration counter is set to zero. Next, the algorithm enters an iterative loop (lines 2-9) that continues until the combined changes in the start times for both controllers fall below a specified threshold θ . This threshold is set to a very small value (e.g., 10^{-9}), ensuring that the algorithm converges only when the start

times have stabilized sufficiently, indicating that the Nash equilibrium has been reached. Within each iteration, the algorithm alternately updates the start times for controllers A and B. Specifically, for controller A, the algorithm seeks to maximize the vote share $S_A(T)$ by adjusting t_a while holding t_b fixed at its current value (line 3). This optimization step identifies the best response for controller A given the current strategy of controller B. Similarly, for controller B, the algorithm minimizes $S_A(T)$ by adjusting t_b while holding t_a fixed at its updated value (line 4). This step determines the best response for controller B, considering the updated strategy of controller A. To ensure stable convergence, an adaptive learning rate μ is used, which is inversely proportional to the iteration count ($\mu = 1/i$). This decreasing learning rate reduces the magnitude of adjustments as the algorithm progresses, helping to avoid oscillations and overshooting. The changes in start times (Δt_a and Δt_b) are computed after each update (lines 5-6), and the iteration counter is incremented (line 7). The loop continues until the changes in start times are negligible, indicating that further adjustments will not significantly affect the vote shares. Once convergence is achieved, the algorithm outputs the Nash equilibrium start times for controllers A and B (t_a^{NE} and t_b^{NE}), along with the corresponding vote share $S_A(T)$ at time T (lines 10-12). At this point, neither controller can improve their outcome by unilaterally changing their strategy, consistent with the definition of a Nash equilibrium.

3. Heterogeneous Mean-field Analysis

Before exploring strategy optimization, we first focus on our objective of understanding how opinions spread in complex networks under temporal control. This understanding requires analyzing the complex voter dynamics described in Eq. (1). However, obtaining full analytical solutions proves challenging due to two key factors: the system's large degree of freedom, which scales with network size, and the time-variant terms introduced by control gains. To obtain an analytical estimate of vote-share trajectories of nodes, we take the heuristics called heterogeneous mean-field theory to investigate the complex dynamical processes of Eq. (1) in the context of competing against a constant opponent. This theoretical approach simplifies our analysis by assuming that agents with the same network degree exhibit statistically equivalent dynamics. Such an assumption proves particularly effective for degree-uncorrelated networks, where no assortative or dis-assortative mixing occurs [27]. Through this analysis (detailed derivations can be found in Appendix B), we obtain the probability of nodes with degree k adopting opinion k at time k (k) and the corresponding vote share (k):

$$x_k(t) = \frac{a_k \alpha - \beta k + \frac{ke^{\alpha t}(\beta + \alpha x_k(t_a))}{\alpha + 1}}{\alpha (a_k + b_k + k)} - e^{-t} \left(\frac{a_k \alpha - \beta k + \frac{k(\beta + \alpha x_k(t_a))}{\alpha + 1}}{\alpha (a_k + b_k + k)} - x_k(t_a) \right),$$

$$S_A(t) = \sum_k p_k x_k(t),$$

$$(10)$$

where

$$\alpha = \sum_{k} \frac{k^{2} p_{k}}{\langle k \rangle} \frac{1}{k + a_{k} + b_{k}} - 1,$$

$$\beta = \sum_{k} \frac{k p_{k} a_{k}}{\langle k \rangle} \frac{1}{k + a_{k} + b_{k}},$$

$$\gamma = \sum_{k} \frac{k^{2} p_{k}}{\langle k \rangle} \frac{1}{k + b_{k}} - 1,$$

$$x_{k}(t_{a}) = x_{0} e^{-t_{a}} + \frac{k}{k + b_{k}} x_{0} \left(e^{\gamma t_{a}} (1 - e^{-t_{a}}) \right).$$
(11)

Here, a_k and b_k stand for allocations to nodes with degree k from controllers A and B, p_k is the fraction of nodes with degree k, $\langle k \rangle = \sum_k k p_k$ is the average degree of the network, and $x_k(t_a)$ is the probability of nodes of degree k holding opinion A at time t_a . Note that, Figs. 4 (c)(d) in Section 4.3.1 have validated our theoretical predictions of vote shares derived from the heterogeneous mean-field analysis in Eq. (10). These figures show that the mean-field approximations closely match the results obtained from direct numerical simulations using Runge-Kutta integration by accurately capturing the dependence of vote shares $S_A(T)$ on starting times in scale-free networks. This agreement demonstrates the reliability of our analytical framework.

Research by Brede et al. [10] suggests that a node's equilibrium dynamics are influenced by its degree. For instance, hub nodes typically exhibit slower equilibration. This slow response adversely impacts their ability to influence the overall vote share effectively over short time intervals. This insight leads us to consider how the inherent timescales of equilibrium within a network affect the strategic allocation of budgets over different periods. Consequently, our research focuses on analyzing how equilibration dynamics vary across networks with diverse levels of heterogeneity. We approach this by examining relaxation times, as characterized by Son et al. [51]. Here, to quantify relaxation times for nodes of degree k, we introduce a normalized order parameter, defined as follows:

$$r_k(t) = \frac{x_k(t) - x_k(\infty)}{x(0) - x_k(\infty)}.$$
(12)

Then, the mean relaxation times for each node with degree k can be written as:

$$\tau_{relax,k} = \int_0^\infty r_k(t)dt = \int_0^\infty \frac{x_k(t) - x_k(\infty)}{x(0) - x_k(\infty)}dt \tag{13}$$

Building on the mean-field solutions outlined in Eq. (10), and assuming a uniform initial state across nodes $(x(0) = x_0)$, we derive an expression to calculate the mean relaxation time for each node with degree k under the heterogeneous mean-field assumption:

$$\tau_{relax,k} = \frac{\alpha \left(\alpha x_0 (a_k + b_k + k) - a_k \alpha + \beta k - k x_0\right) - \beta k}{\alpha \left(\alpha x_0 (a_k + b_k + k) - a_k \alpha + \beta k\right)}.$$
(14)

Incorporating the values of α and β from Eq. (10) into Eq. (14) results in a complicated expression. To facilitate understanding of how equilibration times depend on node degree, we simplify Eq. (14) in the limit of $\frac{a_k+b_k}{k}\ll 1$. Under this condition, we perform a second-order Taylor expansion. The resulting approximation is as follows:

$$\tau_{relax,k} \simeq \frac{\alpha - 1}{\alpha} + \frac{a_k(x_0 - 1) + b_k x_0}{\beta + \alpha x_0} k^{-1} - \alpha \left(\frac{a_k(x_0 - 1) + b_k x_0}{\beta + \alpha x_0} \right)^2 k^{-2} + O\left(\frac{1}{k}\right)^3.$$
(15)

In particular, if controller A and controller B target all nodes equally, i.e. $a_k = a$ and $b_k = b$, we have:

$$\beta + \alpha = -\frac{b}{a}\beta. \tag{16}$$

As β is strictly positive and the sum of α and β is negative, we obtain that α is negative as well. Therefore, we have

$$\frac{a_k(x_0 - 1) + b_k x_0}{\beta + \alpha x_0} = \frac{x_0(a + b) - a}{\frac{x_0(a + b) - a}{a + b}\alpha} = \frac{a + b}{\alpha} < 0.$$

Eq. (15) can now be simplified to:

$$\tau_{relax,k} \simeq \frac{\alpha - 1}{\alpha} + \frac{a + b}{\alpha} k^{-1} - \frac{(a + b)^2}{\alpha} k^{-2} + O\left(\frac{1}{k}\right)^3,\tag{17}$$

which indicates that the approximation of average relaxation times for nodes with degree k is independent of the initial state if both controllers target all nodes uniformly. Notably, the dependence of $\tau_{relax,k}$ on k primarily emerges from two terms. The first term $\frac{\alpha-1}{\alpha}$ establishes a baseline influence. The second term $\frac{a+b}{\alpha}k^{-1}$ shows a linear decay. This term has a negative coefficient $\frac{a+b}{\alpha}$, which suggests an inverse relationship: higher-degree nodes have longer relaxation times. Additionally, the quadratic term $\frac{(a+b)^2}{\alpha}k^{-2}$ acts as a moderating factor. It reduces the variation in relaxation times among nodes with different degrees.

Datasets	Congress votes [52]	Facebook [21]	Advogato [38]	Wikipedia Elections[31]	Twitter[32]
Network Size (N)	219	3862	6541	7118	22322
Number of Edges (V)	764	87324	51127	103689	31823
Average Degree $(\langle k \rangle)$	7.0	45.2	15.6	29.1	2.9
Degree Exponent (λ)	≈ 1.9	≈ 1.6	≈ 1.7	≈ 1.5	≈ 4.3

Table 1

Statistical properties of the real-world datasets used in this study. The datasets span diverse domains, including political discourse (Congress votes), social interactions (Facebook, Twitter), trust networks (Advogato), and voting behavior (Wikipedia Elections). N denotes the number of nodes, |V| is the number of edges, $\langle k \rangle$ represents the average degree, and λ is the degree exponent estimated using the method given in [43]. Data sources are cited for each dataset.

4. Experimental Results

In this section, we focus on investigating how network heterogeneity affects influence propagation dynamics and optimization strategies under temporal control. Specifically, we begin with an overview of our experimental framework in Section 4.1, including the datasets, network structures, and experimental parameters essential for context and reproducibility. Building on this foundation, Section 4.2 analyzes how node degree and network heterogeneity influence system relaxation times—the periods required for systems to reach equilibrium. This analysis reveals crucial insights into the relationship between network structure and transient dynamics, providing the theoretical basis for developing timing-sensitive influence strategies. Then, Sections 4.3.1-4.3.3 evaluates the effectiveness of both uniform and agent-specific optimization approaches within a constant-opponent framework. Finally, in Section 4.3.4, we examine the optimal strategies in a game-theoretical setting where both controllers actively compete against each other.

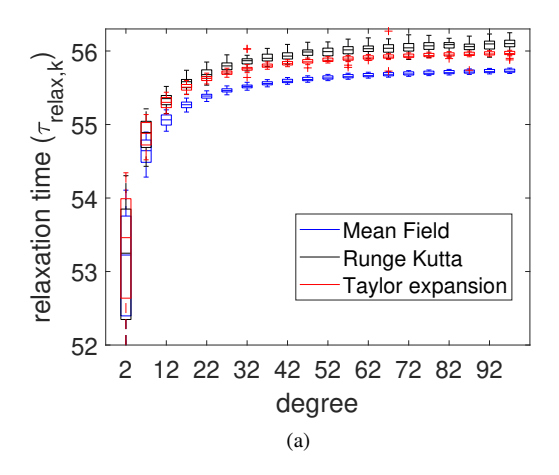
4.1. Dataset Description and Experimental Setup

To validate our theoretical findings and evaluate temporal control strategies, we conduct extensive experiments using both synthetic and real-world networks. For synthetic networks, we employ the configuration model [15], which serves as a standard null model for testing analytical solutions and examining the effects of power-law degree distributions. These networks follow a distribution $p_k \propto k^{-\lambda}$, where k represents the node degree and λ is the degree exponent. More details on the network generation process and choice of network parameters are provided in Appendix C. In addition to synthetic networks, we complement our analysis with experiments on five established real-world networks. These datasets include Congress votes [52], representing mentions between U.S. politicians with edges indicating supportive or opposing references; Facebook [21], a social network among users affiliated with a specific corporation; Advogato [38], a trust network where nodes represent users and edges signify trust relationships; Wikipedia Elections [31], a voting network where nodes correspond to users and edges represent votes (positive or negative) between them; and Twitter [32], a network capturing user-following relationships. The properties of these datasets, including network size, number of edges, average degree, and degree exponent, are summarized in Table 1. By comparing the results from both synthetic and real-world networks, we aim to demonstrate the general applicability and robustness of our methods across diverse settings.

To ensure consistency, we initialize the opinion states uniformly at 0.5 unless specified otherwise, which represents a neutral starting point. Additionally, we conduct experiments across different time horizons: T=16 for analyzing short-term influence dynamics and T=256 for studying long-term equilibrium behavior. For fair comparisons across networks of varying sizes, the control gains are normalized by network size. All simulations are performed using the 4th-order Runge-Kutta method with a time step of 0.01, which ensures both numerical accuracy and computational efficiency.

4.2. Impact of Network Heterogeneity on Relaxation Times

To validate our theoretical findings in Section 3, we first perform detailed numerical experiments to compare the relaxation times $\tau_{relax,k}$ for nodes with degree k using three methods: direct integration via the Runge-Kutta method, mean-field approximations (Eq.(14)), and Taylor expansions (Eq.(17)). Here, direct Runge-Kutta integration serves as the ground truth. It is obtained by numerically solving the original, non-approximated system dynamics described in Eq. (1) to compute the vote-share trajectories $x_i(t)$, and then nodes are grouped by their degree k to calculate average relaxation times via Eq. (13). The corresponding results are displayed in Fig. 2 (a), which shows a consistent increase



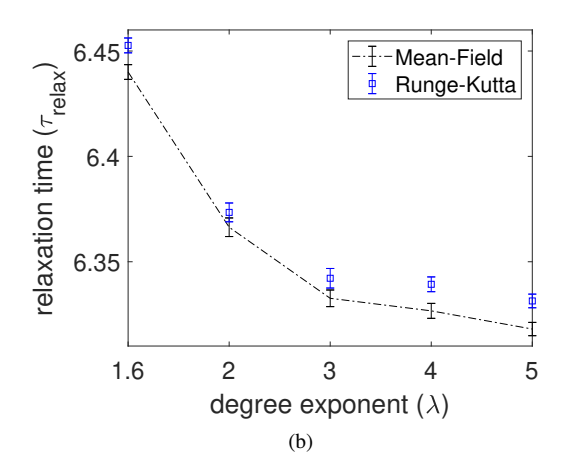


Figure 2: Results for networks with $N=10^4$ nodes and an average degree of $\langle k \rangle=10.5$ averaged over 100 realizations. Controllers A and B initiate resource allocation at time 0 with magnitudes of 0.1 and 1 per node per unit time for Fig. 2 (a) and Fig. 2 (b), respectively. Fig. 2 (a) presents the relationship between the degree k and the relaxation time $\tau_{relax,k}$. Here, $\tau_{relax,k}$ is calculated using direct integration with a Runge-Kutta method (black boxes), a mean-field estimate derived from Eq. (14) (blue boxes), and a Taylor series expansion of Eq. (17) (red boxes) in k up to the second order for networks with an exponent of 1.6. Data are presented as box plots displaying the median, 25th and 75th percentiles, with whiskers extending to the extreme values. Fig. 2 (b) explores how overall average relaxation time τ_{relax} varies with network heterogeneity. Here, we compare τ_{relax} calculated via direct integration with a Runge-Kutta method (blue), and the mean-field approximation (black). Error bars reflect 95% confidence intervals.

in x_k with the node degree k for all the methods. This trend aligns with the Gershgorin circle theorem [17]. According to the theorem, the eigenvalues of nodes, are situated within discs. Each disc's radius, computed as $-1 + \frac{1}{1 + \frac{a_k + b_k}{2}}$ is

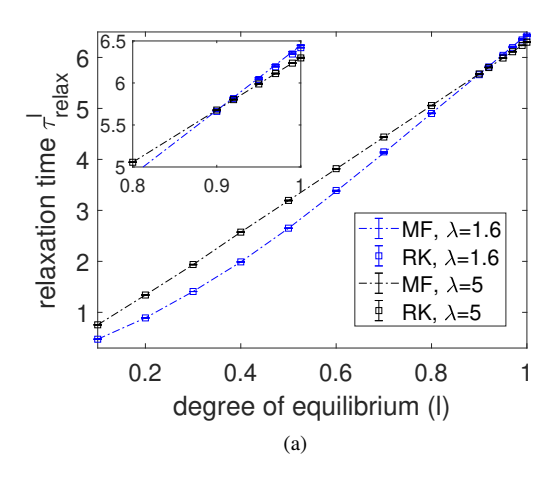
centered at zero. As node degree k increases, the term $\frac{a_k+b_k}{k}$ decreases, leading to a reduction in the radius of the disc. This smaller radius implies a tighter clustering of eigenvalues around zero, which in turn indicates longer relaxation times for nodes with higher degrees. Additionally, Fig. 2 (a) indicates that the estimates of $\tau_{relax,k}$ derived from the mean-field method and Taylor expansion align closely with the direct integration, validating the theoretical prediction in Section 3 that nodes with higher degrees exhibit longer relaxation times.

In the following, we use the overall average relaxation time τ_{relax} to quantify network's natural timescales towards equilibrium under uniform targeting. τ_{relax} is calculated using a weighted average where the relaxation time $\tau_{relax,k}$ of nodes with degree k contributes proportionally to their frequency p_k , written as:

$$\tau_{relax} = \sum_{k} p_{k} \tau_{relax,k} = \sum_{k} p_{k} \frac{k (\beta(a+b)+a) + \beta(a+b)^{2}}{\beta(a+b)(a+b+k)}$$

$$\simeq \sum_{k} p_{k} \left(\frac{\langle k \rangle \left(k(a+b) - (a+b)^{2} - k^{2} \right)}{k^{2}(a+b) \left(\sum_{k} \frac{p_{k}}{k} (a+b) - 1 \right)} + 1 \right) + O\left(\frac{1}{k}\right)^{3}$$
(18)

Our next aim is to analyze how network heterogeneity, characterized by the degree exponent λ , affects overall average relaxation times τ_{relax} . To achieve this, we compute the average relaxation time τ_{relax} across various λ settings. Fig. 2 (b) displays the dependence of τ_{relax} on network heterogeneity λ . We again compare the values of τ_{relax} obtained via Runge-Kutta integration, which serves as the ground truth, with the theoretical estimates from Eq. (18). The results in Fig. 2 (b) confirm that the simulation and theoretical estimates align well. Moreover, the trend of dependence of τ_{relax} on network heterogeneity λ indicates that networks with more heterogeneity have longer timescales to reach equilibrium. By integrating this observation with that from Fig. 2 (a), it becomes evident that the extended timescales observed in networks with high degrees of heterogeneity predominantly originate from nodes with higher degrees.



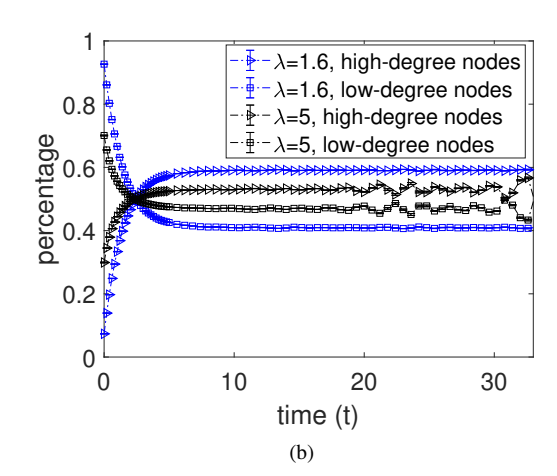


Figure 3: Results for networks with $N=10^4$ nodes and an average degree of $\langle k \rangle = 10.5$. Error bars represent 95% confidence intervals across 100 realizations. Both controllers A and B initiate resource allocation at time 0 with magnitudes of 1 per node per unit time. The legends $\lambda=1.6$ or $\lambda=5$ correspond to power-law distributions $P(k) \propto k^{-1.6}$ or $P(k) \propto k^{-5}$, respectively. Panel (a) of Fig. 3 explores the dependence of relaxation times τ^l_{relax} on degree of equilibrium l for different levels of network heterogeneity $\lambda=1.6$ and $\lambda=5$. Here, we compare the results calculated by direct integration using the Runge-Kutta method (labelled as RK) and the mean-field approximation (labelled as MF). Panel (b) of Fig. 3 presents the evolution of average vote share changes in proportion. It distinguishes between "low-degree nodes", which represents the first 80% of nodes, and "high-degree nodes", which represents the top 20%. The y-axis measures the proportion of average state changes in these groups relative to the total changes.

In the previous discussion, τ_{relax} represents the timescale for reaching equilibrium. However, our interest extends to the timescales associated with approaching non-equilibrium states. To address this, we introduce a new metric termed the *degree of equilibrium l*. This metric quantifies the progress toward equilibrium as a fraction of progress towards the equilibrium state, measured by $l = \frac{|S_A(T) - S_A(0)|}{|S_A(\infty) - S_A(0)|}$. Here, $S_A(0)$ represents the initial vote share, and $S_A(\infty)$ is the vote share at equilibrium. We then define the average timescale for approaching $lS_A(\infty)$ as the *l-percentage relaxation time*, τ_{relax}^l , calculated with the integral:

$$\tau_{relax}^{l} = \int_{0}^{t'} r(t)dt = \int_{0}^{t'} \sum_{k} p_{k} r_{k}(t)dt$$
 (19)

where t' is the time at which the vote shares satisfy $S_A(t') = lS_A(\infty) + (1-l)S_A(0)$. The expression quantifies the average timescale at which the system's vote-share dynamics reach the specified l-percentage of the equilibrium vote share.

We then investigate how different levels of network heterogeneity λ and the degree of equilibrium l influence the l-percentage relaxation times τ^l_{relax} , as defined in Eq. (19), and present these results in Fig. 3 (a). The relaxation time τ^l_{relax} , in this context, refers to the time it takes for the system to reach a certain percentage (l) of its equilibrium state. Understanding how this relaxation time varies with network heterogeneity provides insights into the temporal dynamics of influence propagation in complex networks.

In Fig. 3 (a), we observe the relationship between network heterogeneity and the l-percentage relaxation times. Specifically, when l values are low—indicating that the system is far from equilibrium—networks with lower heterogeneity (higher λ values) exhibit longer l-percentage relaxation times compared to more heterogeneous networks (lower λ values). This suggests that in the early stages of the dynamics, less heterogeneous networks take longer to progress towards equilibrium. The initial delay in these networks may be due to the uniform distribution of connections, which results in a more gradual propagation of influence. However, as l increases and the system approaches equilibrium, this pattern reverses: more heterogeneous networks begin to show longer relaxation times. This reversal in behavior, highlighted in the inset of Fig. 3 (a), indicates that the structure of more heterogeneous networks causes a slowdown as they near equilibrium. This can be attributed to the presence of high-degree nodes

(hubs) in these networks, which require more time to align their state with the rest of the network, thereby delaying the overall system's approach to equilibrium.

This crossover behavior suggests a two-stage process in the dynamics of heterogeneous networks as they approach equilibrium. Initially, low-degree nodes, which are more numerous, drive the changes due to their relative ease of influence. As the system moves closer to equilibrium, the influence of high-degree nodes becomes more pronounced. To support this hypothesis, we present Fig. 3 (b), which tracks the evolution of average vote share changes over time, distinguishing between low-degree and high-degree nodes.

In Fig. 3 (b), we classify the first 80% of nodes as low-degree and the remaining 20% as high-degree, following the Pareto principle. We then calculate the rate of state change $\frac{dx_i}{dt}$ for both groups by summing the rates within each group and normalizing these rates by the number of nodes in each group. This approach allows us to compare the average impact of low-degree and high-degree nodes on the overall changes in vote shares, providing a more detailed understanding of the network's dynamics.

The results in Fig. 3 (b) provide clear evidence of the shifting dynamics between these two groups. Initially, low-degree nodes contribute the most to vote-share changes, especially in networks with high heterogeneity (low λ). This is likely because the influence propagates more quickly through the numerous low-degree nodes. As time progresses and the system nears equilibrium, high-degree nodes increasingly dominate the vote-share changes. This transition is more pronounced in highly heterogeneous networks, where the initial influence of low-degree nodes is more significant compared to their influence in less heterogeneous networks. Over time, the high-degree nodes in these highly heterogeneous networks take over as the primary drivers of change, accounting for a larger proportion of the total vote-share changes.

By combining the results from Figs.3 (a) and 3 (b), we gain a comprehensive understanding of the dynamics. For small values of l, the changes in vote shares are primarily driven by low-degree nodes, as shown in the early part of Fig.3 (b). In this phase, highly heterogeneous networks, which contain many low-degree nodes, reach the desired states more quickly than less heterogeneous networks. Conversely, for large l, high-degree nodes become the key contributors to the changes in vote shares. Networks with a high degree of heterogeneity have more high-degree nodes, which tends to delay reaching equilibrium due to the more complex dynamics associated with these influential nodes.

These insights into the relaxation dynamics are crucial as they highlight the dual role of network heterogeneity in shaping the speed and pattern of influence spread. In the initial phase, low-degree nodes in highly heterogeneous networks facilitate rapid early changes, making them important targets for early-stage influence efforts. However, as the system approaches equilibrium, the role of high-degree nodes becomes more pronounced, especially in highly heterogeneous networks where their influence can slow down the final convergence to equilibrium. Understanding this two-stage process will inform our investigation of optimal resource allocations in the next section, as it underscores the importance of timing and targeting in influence strategies.

4.3. Analysis of Optimal Strategies

In the previous sections, we have validated our theoretical analysis and gained insights into voting dynamics, particularly how network heterogeneity and time horizons influence optimal campaign timing. Building on these findings, in this section, we focus on our second objective of evaluating the performance of inter-temporal optimization strategies across various settings. Section 4.3.1 explores the effects of time horizons and relative budgets on optimal starting times under constant-opponent settings, followed by a comparison with individual optimization strategies in Section 4.3.2. Section 4.3.3 further extends the analysis by incorporating agent heterogeneity. Finally, in Section 4.3.4, we investigate inter-temporal control strategies in a game-theoretical setting.

4.3.1. Optimal Strategies in the Constant-opponent Setting with Same Starting Time

We start with finding the optimal strategies in the simple scenario described in Section 2.1, where controller A only has the flexibility to determine when to start control, and once started, it has to target all nodes equally. Specifically, we obtain the optimal starting time of controller A by interior-point optimization when controller B starts its control from time t=0 under equal budgets. First, in order to have an intuition of how the optimal starting time affects the vote shares regarding network heterogeneity, we depict the evolution of vote shares for networks with degree exponents $\lambda=1.6$ and $\lambda=5$ within two very different time horizons T=16 and T=256 in Figs. 4 (a) and (b) respectively. The choice of time horizons T=16 and T=256 allows us to investigate two scenarios: One where there is enough time for the network to approach the equilibrium state T=256 and one where the campaign ends before reaching

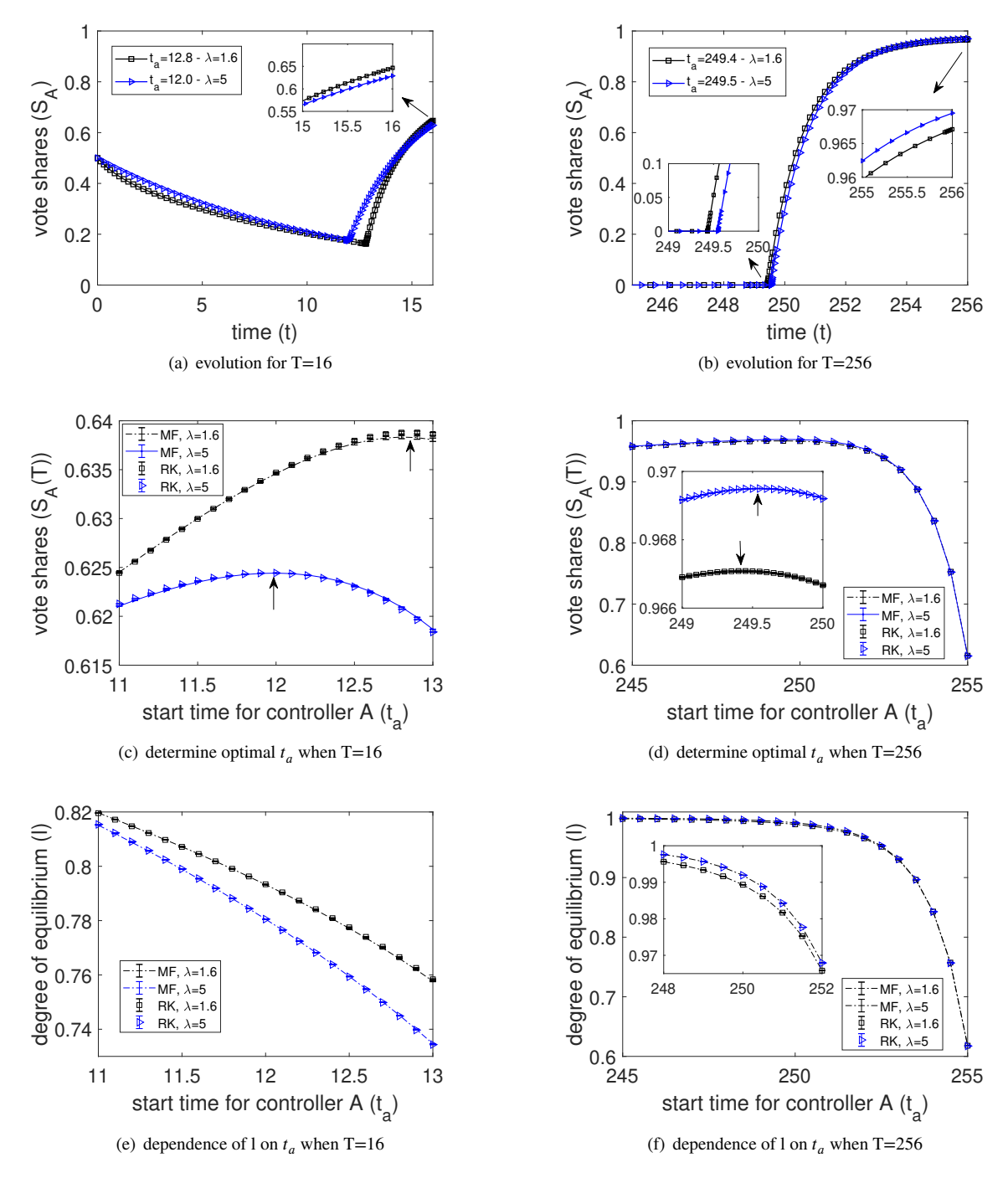
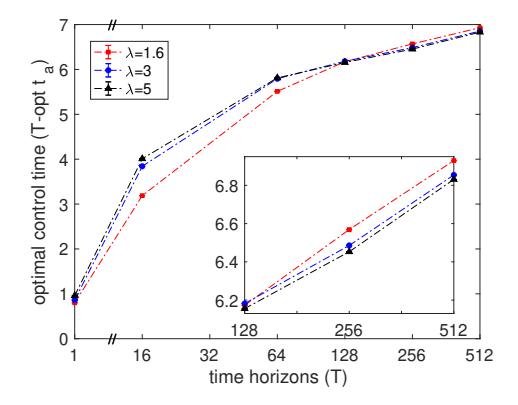


Figure 4: Figs. (a) and (b) illustrate the evolution of total vote shares under optimal control by controller A for time horizons of T=16 and T=256, respectively. The turning points in these figures mark when controller A initiates optimal control. Figs. (c) and (d) explore how the timing of controller A's control start affects vote shares for T=16 and T=256, respectively. Figs. (e) and (f) examine how the degree of equilibrium I varies with the starting time of the A controller I. To determine the optimal starting timing, networks must balance the budget per node with the degree of equilibrium. Results are based on networks with I0 nodes and an average degree I1 nodes are time 0 in all cases. Black squares represent networks with a degree exponent I1 nodes with I2 nodes and an average degree I3 nodes are time 0 in all cases. Black squares represent networks with a degree exponent I3 nodes are time 0 in all cases. Black squares represent networks with a degree exponent I3 nodes are time 0 in all cases.



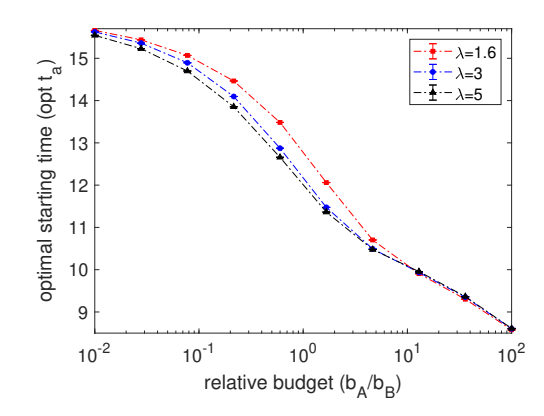


Figure 5: Fig. (a) shows how the optimal effective control time of controller A $(T-optt_a)$ varies with network heterogeneity and time horizons. In this scenario, the control gains of controller B for each node are fixed at 1 per unit time starting from time 0. controller A's total budgets are aligned with those of controller B; for instance, when T=10, b_A and b_B are both set to $N\times T$. The y-axis measures the difference between the time horizon and the optimized t_a . Fig. (b) explores the relationship between the optimal starting times of controller A (optt_a) and network heterogeneity, along with varying budget ratios. Here, the time horizon is fixed at T=16. Similar to Fig. (a), controller B's control gains remain constant at 1 per unit time from the start. The total budget of controller A is presented as a ratio to controller B's budget, which is depicted on the x-axis. This analysis is conducted on networks with $N=10^4$ nodes and an average degree $\langle k \rangle$ of 10.5, with results aggregated from 100 realizations. The curves represent networks with different power law exponents, where $\lambda=1.6$ on the legend corresponds to a power law distribution exponent 1.6. Initial opinion states are set to 0.5 for all nodes in each case. Error bars represent 95% confidence intervals.

equilibrium (T = 16). Further, the turning points where vote shares change dramatically in Figs. 4 (a) and (b) indicate the optimal times for controller A to start control.

We make the following observations. First, we note from Fig. 4 (a) that the optimized controller for networks with degree exponent $\lambda=1.6$ will start later than for networks with degree exponent $\lambda=5$ for the short time horizon T=16. Additionally, at the very beginning of the competition, vote shares for networks with degree exponent $\lambda=1.6$ decline slightly faster, which roughly indicates that highly heterogeneous networks respond more quickly to the resource injection in the early stage. Second, in Fig. 4 (b) we show the evolution of vote shares under the optimized control for a long time horizon T=256. We also note here that compared with networks with degree exponent $\lambda=5$, the optimized controller for networks with degree exponent $\lambda=1.6$ has to start slightly earlier (see inset). Moreover, vote shares for networks with degree exponent $\lambda=1.6$ have been slightly exceeded at the end of the competition by networks with degree exponent $\lambda=5$. Given that for both networks, the vote shares when controller A starts control are the same (i.e., $S_A(t_a)=0$), the changes in vote shares can only be a result of budgets and the network response speed.

To demonstrate the accuracy of interior-point optimization, we also present the relationship between vote shares and the starting times of controller A in Figs. 4 (c) and (d). These figures display a convex curve that peaks at the optimal starting times, indicated by arrows. Note that, these peak values are consistent with the turning points shown in Figs. 4 (a) and (b). This peak in the curves represents a balance of two competing factors. On the one hand, an early start for controller A (i.e., when t_a is small) allows more time for network influence but with limited resources per node per unit time. This extended period of influence helps the system move closer to equilibrium by increasing l. However, the sparse resource allocation results in smaller final vote shares, which decreases S_A . On the other hand, a later start provides controller A with more resources per node, enhancing the final vote share. However, this approach reduces the time available for exerting influence on the network. Thus, the optimal starting time strikes a balance between maximizing resources per node and allowing sufficient time for their effective deployment.

To proceed, we move on to investigating the dependence of the optimized starting times on time horizons T and relative budgets b_A/b_B . To this end, Fig. 5 (a) illustrates the dependence of optimal control times $(T-optt_a)$ on network heterogeneity and time horizons. Generally, the optimized controller reserves its budget until the campaign's latter stages. Initially, the system is influenced solely by the opponent's actions. As the campaign deadline approaches, the optimized controller significantly increases its allocations. This abrupt shift is evident from the sudden increase in

vote shares shown in Figs. 4 (a) and (b). Moreover, as illustrated in Fig. 5 (a), the timing of optimal control varies with network structure. In more detail, for shorter time horizons, optimal control times tend to start later in networks with high heterogeneity (indicated by smaller λ values). Conversely, in the case of longer time horizons, it's beneficial for control to commence earlier in these networks. This pattern can be explained from earlier observations in Fig. 3 (a). At the end of shorter campaigns, the network is far from equilibrium, characterized by a low equilibrium degree l. This state is primarily influenced by nodes with low degrees, which equilibrate more quickly. Hence, more heterogeneous networks, which typically have many low-degree nodes, react faster to resource allocations, and lead to a later start for short campaigns. On the other hand, for longer campaigns, as the network approaches a higher degree of equilibrium $(l \to 1)$, more heterogeneous networks exhibit slower response times due to larger inherent relaxation times, which necessitates an earlier start for effective control.

To validate our conclusion, we analyze the degree of equilibrium achieved with optimized control for different time horizons: T=16 and T=256, as illustrated in Figs. 4 (e) and (f) respectively. Specifically, Fig. 4 (e) indicates that for a short time horizon of T=16, the degree of equilibrium never exceeds 0.82. Additionally, Fig. 3 (a) reveals that when the degree of equilibrium l is below 0.9, highly heterogeneous networks have shorter relaxation times τ_{relax}^l compared to less heterogeneous ones. Consequently, in such networks, the rapid response to control allows for a later start in the application of optimized strategies. Conversely, with longer time horizons, as shown in Fig. 4 (f), the degree of equilibrium approaches 1. Under these conditions, less heterogeneous networks adapt more swiftly to control measures. This faster response enables optimal control strategies for these networks to start later.

Fig. 5 (b) shows the dependence of the optimal starting times of the targeting controller on network heterogeneity and relative budgets. In this figure, we observe that, when the optimized controller is in resource superiority, it will start earlier than if it is in a budget disadvantage. Moreover, network heterogeneity leads to slight differences between starting times under the same control settings when relative budgets are not extremely small or large.

In addition to analyzing synthetic networks with controlled network heterogeneity, we extend our investigation of inter-temporal control to diverse real-world networks. As shown in Table 1, these networks exhibit substantially different structural properties, ranging from sparse to dense connectivity patterns and varying degrees of network heterogeneity. In Table 2, we present a comprehensive comparison between two strategies of controller A: one using optimized inter-temporal allocations and another starting at time 0. For each network, we evaluate the optimized starting times (Opt t_a) and compare the resultant vote shares (Opt S_A) with the baseline scenario where controller A begins targeting agents from time 0 (S_A for $t_a = 0$). To ensure robustness, we conduct this analysis across different time horizons ($T = \{16, 256\}$) and budget ratios ($b_A/b_B = \{0.1, 1, 10\}$). Despite the significant variations in network size, average degree, and degree exponent among these real-world networks (as detailed in Table 1), the results in Table 2 demonstrate that our optimization strategy consistently outperforms the baseline across all network topologies. For example, in the Congress votes network with T = 16, optimizing the starting time yields an improvement in vote share from 0.5 to 0.7 when $b_A/b_B = 1$. Furthermore, we observe that when the optimized controller possesses resource superiority ($b_A/b_B = 10$), they consistently start earlier than when operating under a budget disadvantage $(b_A/b_B=0.1)$. For instance, in the Congress votes network with T=16, the optimal starting time decreases from 14.730 when $b_A/b_B = 0.1$ to 10.476 when $b_A/b_B = 10$. Similar patterns can be observed across other real-world networks for all time horizons, which demonstrates the alignment with our observations from synthetic networks.

Even though the simplicity of all nodes having the same starting time allows for analytical solutions for vote-share trajectories, we are also interested in obtaining numerical results for a more general scenario in which the controller can assign different starting times and budget allocation for individual nodes. Therefore, in Section 4.3.2, we further investigate the influence-maximizing strategies in the context that nodes can have different starting times and budget allocations by combining optimization schemes with numerical integration of Eq. (1).

4.3.2. Individual Optimization

In the following, we present the numerical results for the individual optimization setting described in Section 2.2 according to Algorithm 1. Here, due to the large parameter spaces involved in individual optimization, we have reduced the size of networks from $N=10^4$ to $N=10^2$ for computational efficiency. Specifically, Fig. 6 (a) evaluates the performance of individual optimization by showing the vote shares achieved by node-specific optimization relative to the baseline scenario where the optimized controller assigns a single starting time for the whole network based on different relative budgets of the controllers $(S_A^{indivi}(T)/S_A^{const}(T))$. From our analysis of Fig. 6, we find that for a small relative budget, a large improvement can be achieved (but note that the improvement is nevertheless small in absolute numbers). In Figs. 6 (b) and (c) we further explain why the individual optimization is more efficient for the small

Network	Control Settings	Performance Metrics		
rection	Control Settings	Opt t _a	Opt S_A	S_A for $t_a = 0$
Congress votes	$T = 16$, $b_A/b_B = 0.1$	14.730	0.248	0.117
	$T = 16$, $b_A/b_B = 1.0$	12.533	0.705	0.500
	$T = 16, b_A/b_B = 10$	10.476	0.958	0.909
	$T = 256$, $b_A/b_B = 0.1$	251.930	0.783	0.091
	$T = 256$, $b_A/b_B = 1.0$	250.025	0.972	0.500
	$T = 256$, $b_A/b_B = 10$	248.060	0.997	0.909
Facebook	$T = 16$, $b_A/b_B = 0.1$	15.295	0.378	0.369
	$T = 16$, $b_A/b_B = 1.0$	13.149	0.531	0.500
	$T = 16, b_A/b_B = 10$	7.897	0.907	0.889
	$T = 256$, $b_A/b_B = 0.1$	251.317	0.389	0.092
	$T = 256$, $b_A/b_B = 1.0$	247.199	0.934	0.500
	$T = 256$, $b_A/b_B = 10$	245.771	0.996	0.909
Advogato	$T = 16$, $b_A/b_B = 0.1$	14.942	0.313	0.233
	$T = 16$, $b_A/b_B = 1.0$	13.085	0.634	0.500
	$T = 16, b_A/b_B = 10$	9.800	0.941	0.906
	$T = 256$, $b_A/b_B = 0.1$	252.239	0.645	0.091
	$T = 256$, $b_A/b_B = 1.0$	248.804	0.960	0.500
	$T = 256, b_A/b_B = 10$	247.780	0.996	0.909
Wikipedia	$T = 16$, $b_A/b_B = 0.1$	14.995	0.378	0.289
	$T = 16$, $b_A/b_B = 1.0$	13.490	0.638	0.500
	$T = 16, b_A/b_B = 10$	9.760	0.920	0.893
	$T = 256$, $b_A/b_B = 0.1$	252.918	0.583	0.091
	$T = 256$, $b_A/b_B = 1.0$	247.588	0.938	0.500
	$T = 256$, $b_A/b_B = 10$	247.356	0.996	0.909
Twitter	$T = 16$, $b_A/b_B = 0.1$	14.752	0.284	0.100
	$T = 16$, $b_A/b_B = 1.0$	12.725	0.738	0.500
	$T = 16, b_A/b_B = 10$	10.594	0.960	0.909
	$T = 256$, $b_A/b_B = 0.1$	252.216	0.810	0.091
	$T = 256$, $b_A/b_B = 1.0$	250.157	0.973	0.500
	$T = 256, b_A/b_B = 10$	248.090	0.997	0.909

Table 2 Comparison of optimized starting times (Opt t_a) and resulting vote shares (Opt S_A) for controller A against baseline scenarios where controller A starts targeting agents from time $t_a=0$ (S_A for $t_a=0$). The analysis is conducted on real-world networks with diverse properties, as detailed in Table 1, and considers different time horizons ($T=\{16,256\}$) and budget ratios ($b_A/b_B=\{0.1,1,10\}$).

budget scenarios. There, we clearly see two regimes for the optimized control gains and starting times under varying relative budgets. For small relative budget ratios, the control gains decrease with the nodes' degree while the starting times increase with the nodes' degree. However, for large relative budget ratios, the opposite holds. Moreover, for small budgets, the optimized controller only targets nodes with small degrees and ignores large-degree nodes. Thus, the optimized controller does not need to waste its resources on nodes that are hard to change states in a short period, and can achieve improvements in the vote shares compared with the non-individual-optimization scenario where the controller has to target all nodes equally. A more detailed exploration of the individual optimization in the special case of $b_A = b_B$ can be found in Appendix D, which shows the convergence of Algorithm 1 and the positive correlation between budget allocations and degree under node-specific control.

In conclusion, by applying individual optimization, we observe that the vote shares can be improved, especially for highly heterogeneous networks. However, we also note that the improvement is consistently very small in relative

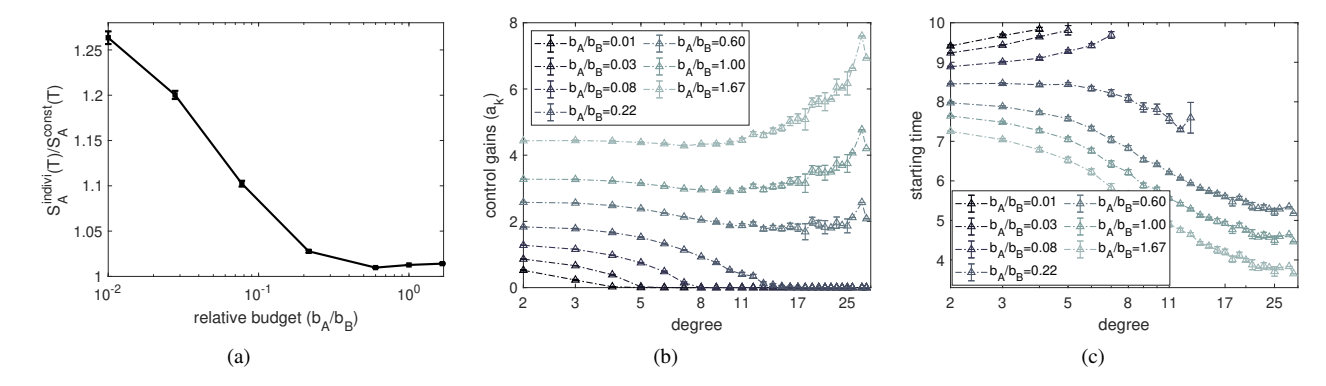


Figure 6: Fig. (a) shows the dependence of average relative vote share $S_A^{indivi}(T)/S_A^{const}(T)$ on relative budgets. Figs. (b) and (c) show the dependence of control gains and starting times by individual optimization on degrees and relative budgets, respectively. All the calculations are based on networks with degree of heterogeneity $\lambda=1.6$. The network size is $N=10^2$ and $\langle k \rangle=6$ and tested in 10 realizations. The control gains of controller B pertaining to each node are all fixed as 1 per unit time from time 0. The time horizon T is set as T=10. The initial states of opinion distribution are 0 for all nodes. Error bars indicate 95% confidence intervals.

numbers for equal or large relative budget settings and very small in absolute numbers for the setting of budget inferiority.

4.3.3. Individual Optimization Considering Agent Heterogeneity

In this section, we further explore the combined effect of the levels of zealotry and degrees on optimal starting times and budget allocations in heterogeneous networks. The model formulation for individual optimization accounting for agent heterogeneity in terms of zealotry levels, are illustrated in Section 2.2.1. For our experiments, we randomly select 20% of the population to become zealots with the same zealotry q, and keep the remaining nodes as normal agents. In Figs. 7 (a)-(d) we show the relationship between optimal budget allocations and nodes' degrees for varying levels of zealotry. We find that, regardless the levels of zealotry, more resources will be allocated to normal agents than to zealots. For example, even for a low level of zealotry q = 0.1, the maximum budget allocation for zealots is less than 20 but it is near to 25 for normal agents. Moreover, from Figs. 7 (a) and (b), we find that, similar to the optimal strategies observed in the complete network (see Appendix E), there are two regimes of optimal strategies for the zealots regarding the levels of zealotry. In more detail, for medium and large levels of zealotry, with increasing degrees, zealots will be allocated fewer resources and start later. However, the opposite holds for small levels of zealotry. Furthermore, in Figs. 7 (c) and (d), we show the optimal budget allocations and starting times for normal agents. We find that, regardless of the different levels of zealotry of zealots, the patterns of the dependence of budget allocations and starting times on nodes' degrees are similar: the larger the node's degree, the larger the budget allocation and the earlier the optimal starting time for normal agents. The positive correlation between nodes' degrees and budget allocations for normal agents regarding different levels of zealotry is also observed by Moreno et al. [41] in a stationary state.

4.3.4. Optimal Strategies in the Game-Theoretical Setting

Similar to the analysis of influence-maximizing strategies in the constant-opponent setting, we start our investigation for optimal strategies in the game-theoretical setting by depicting the evolution of vote shares at Nash equilibria. To fully explore the best responses of both controllers in the case of budget inequality, we start with the context where one of the controllers is in resource superiority. In more detail, Figs. 8 (a) and (b) show the evolution of vote shares for a short time horizon T = 16 in a Nash equilibrium when controller A has a larger budget than controller B. We note that, in both Figs. 8 (a) and (b), controller A always starts earlier than controller B. Given that the initial setup for controller A and controller B is the same except for the budgets, we see that the controller with a budget advantage will start control earlier. Furthermore, a closer inspection of Figs. 8 (a) and (b) gives us an insight into the game played by controller A and controller B to maximize their pay-off functions. In general, the evolution of vote shares can be divided into three stages (see the sequence numbers in Figs. 8). 1) No controller exerts any influence. 2) The first mover changes system states. 3) The second mover starts control and the system is subject to both controllers. In contrast to

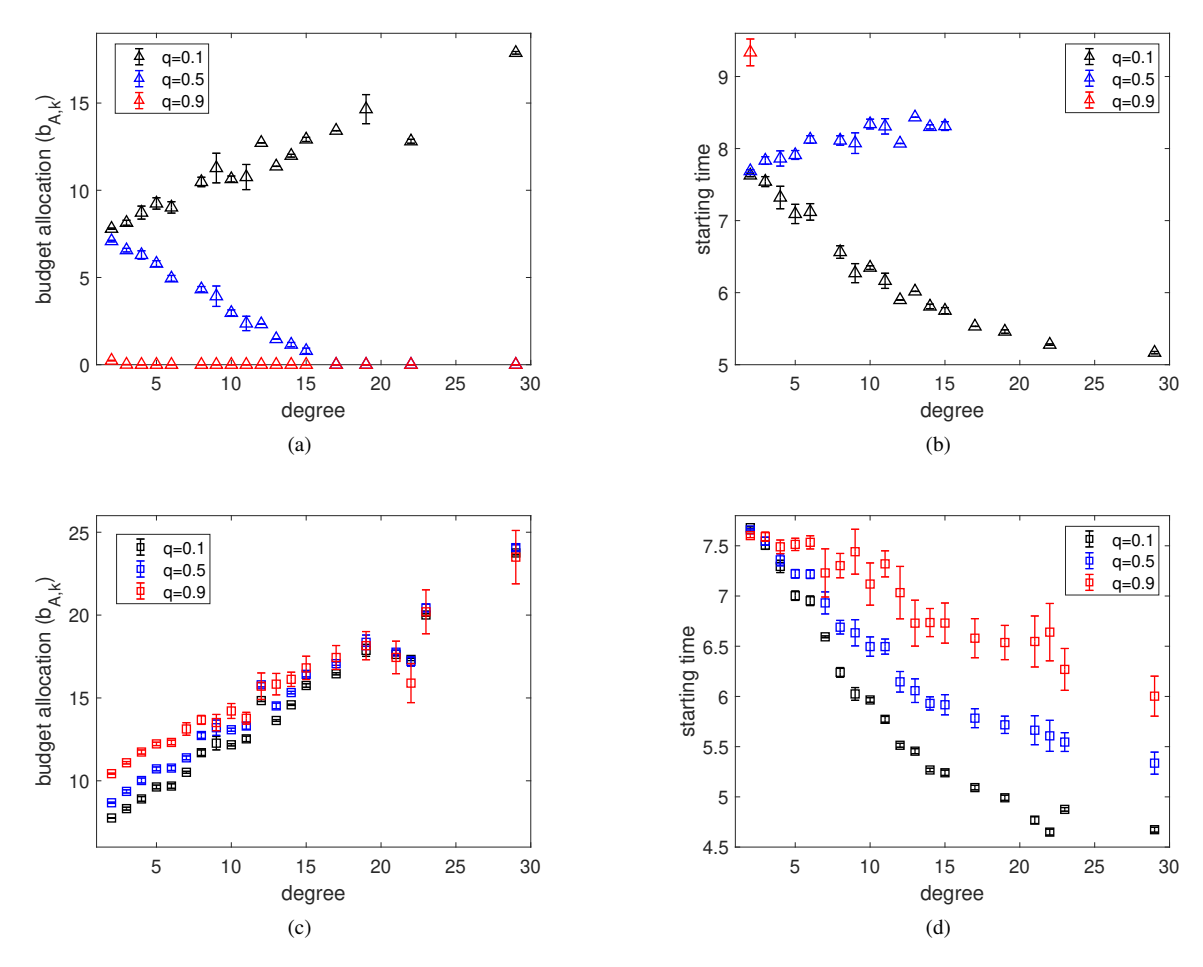
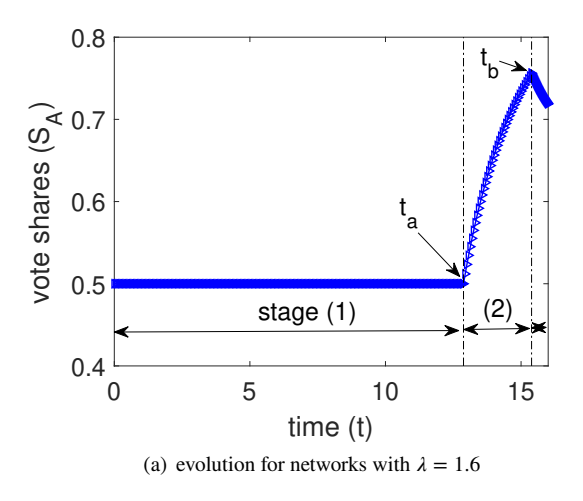


Figure 7: Figs. (a) and (b) show the dependence of budget allocations and starting times on nodes' degrees for varying zealotry obtained by individual optimization for zealots. Figs. (c) and (d) are the dependence of budget allocations and starting times on nodes' degrees obtained by individual optimization for normal agents. Calculations are based on heterogeneous networks with $N=10^2$, $\langle k \rangle=6$, degree exponent $\lambda=1.6$ and tested in 10 realizations. In each realization, we randomly choose 20% population of the network becoming zealots with the zealotry level denoted by q, i.e., 0.1,0.5,0.9. The control gains of controller B pertaining to each node are all fixed as 1 per unit time from time 0. The time horizon T is set as T=10. The initial states of opinion distribution are 0 for all nodes. Error bars indicate 95% confidence intervals.

the vote-share trajectories in the constant-opponent setting where the vote shares increase monotonously when the active controller starts control, we note that there are turning points in the intersection of the second stage and the third stage. In the game-theoretical setting, the controller with budget advantages (i.e., controller A) always starts control first to seize the initiative. In contrast, the other controller will concentrate its resources in the final stage in order to use limited resources more effectively and achieve some pull-back from the other controller's initial advantage (see Figs. 8 (a) and (b)). In addition, by comparing Figs. 8 (a) and (b), we observe that the starting time of the first mover in highly heterogeneous networks tends to be later than in less heterogeneous networks. However, the starting time of the second mover in highly heterogeneous networks is later than that in less heterogeneous networks. These phenomena can be explained by our earlier observations about network's timescales towards equilibria in Section 3. Since, for short time horizons (e.g., T = 16), highly heterogeneous networks respond to the resource allocation faster, the networks with degree exponent $\lambda = 1.6$ tend to start control later compared with networks with degree exponent $\lambda = 5$.

Next, we consider the effect of relative budgets on Nash equilibrium strategies. In Fig. 9(a), we present the optimal starting times of controllers A and B for budget ratios b_A/b_B equal to 0.1, 1, and 10 in networks with varying degrees of heterogeneity, characterized by degree exponents from 1.6 to 5. We make the following key observations: (i) Symmetry



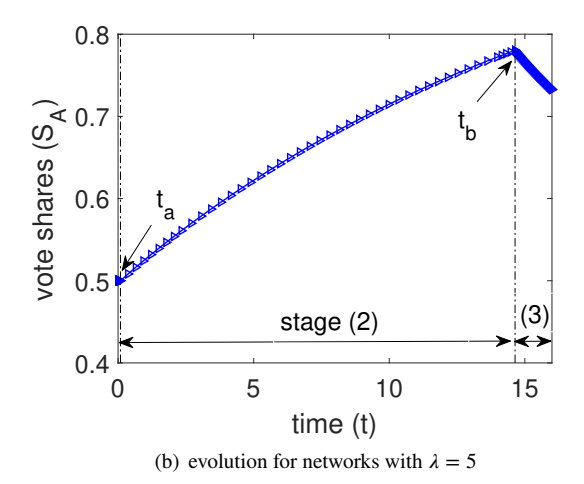
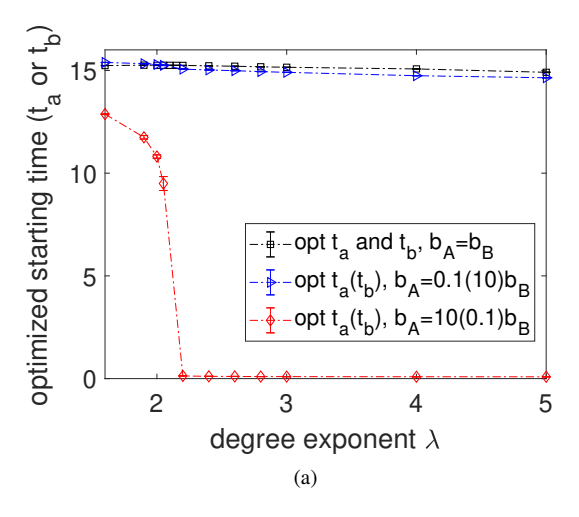


Figure 8: Evolution of total vote shares in the game-theoretical setting. Calculations are based on networks with $N=10^4$ and $\langle k \rangle = 10.5$. The budgets of controller B are $b_B=NT$ and $b_A=10b_B$ for controller A. The initial states of opinion distribution are 0.5 for all nodes and the time horizon is set as T=16. The dotted line distinguishes three stages. t_a and t_b shown by arrows are the solutions for Nash equilibrium. Fig. 8 (a) and Fig. 8 (b) represent the evolution for networks with degree of heterogeneity $\lambda=1.6$ and $\lambda=5$ respectively.



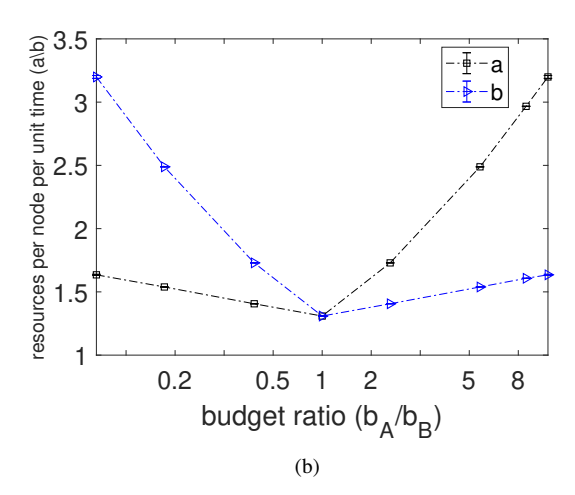


Figure 9: Fig. (a) shows the dependence of starting time at Nash equilibria on network heterogeneity and budgets under the game-theoretical settings. Black squares show the Nash equilibrium strategy for both controller A and controller B in the condition of equal budgets. Blue triangles show the Nash equilibrium strategy for controller A if $b_A = 0.1b_B$ and the Nash equilibrium strategy for controller B if $A = 10b_B$ and the Nash equilibrium strategy for controller A if $A = 10b_B$ and the Nash equilibrium strategy for controller $A = 10b_B$. Fig. (b) shows the dependence of resource allocations on relative budgets. The black and blue lines represent the resources for each node per unit time allocated by the controller $A = 10b_B$ and $A = 10b_B$ respectively. Calculations are based on networks with $A = 10^4$ and $A = 10^4$ and A = 1

in Nash equilibrium starting times: Due to the symmetry of the game played by controllers A and B, we have merged the optimal starting times of controller A in the setting of $b_A/b_B=0.1$ and that of controller B in $b_A/b_B=10$ (see the blue line in Fig.9(a)). Similarly, the optimal starting time of controller A in $b_A/b_B=10$ is identical to that of controller B under $b_A/b_B=0.1$, represented by a single red line in Fig.9(a). (ii) Effect of network Heterogeneity: There is a jump in the optimal starting times of the controller with a budget advantage for networks with degree exponents around 2.2.

Specifically, when degree exponents are greater than 2.2, the controller with a budget advantage will start control from the very beginning of the campaign. Otherwise, it will use its budget closer to the end of the campaign. Moreover, for a short time horizon (e.g., T=16), controllers in highly heterogeneous networks will start later, as indicated by the monotonically decreasing curves. This behavior is consistent with the results observed in the constant-opponent case. (iii) Effect of budget inequality: By comparing the optimal starting times in scenarios of budget inequality, it becomes clear that the controller with a budget advantage will always start earlier compared to the controller with a lower budget.

We further explore the dependence of allocation per node on the budget ratio in Fig. 9 (b). It is clear that, although the controller with budget advantages tends to start earlier, it allocates more resources on each node per unit time as well. Therefore, for stage (3) in Figs. 8 (a) and (b), the second mover can only buffer the increase of S_A , it is impossible for the second mover to gain a larger vote share than the first mover.

Similar to Section 4.3.2, we can apply the individual optimization in the game-theoretical setting. However, as the individual optimization only has small improvements in the absolute value of vote shares, we do not further investigate it in the game-theoretical setting.

5. Conclusion

This study presents a comprehensive investigation of the influence maximization problem from the perspective of inter-temporal budget allocations in the voter model. By relating IM to network control and integrating time information into opinion dynamics, we explore optimal campaign strategies within limited time horizons, considering competing controllers and agent heterogeneity.

Our study makes several contributions to the field of transient control in voting dynamics, building upon and advancing prior work in this area. First, we provide a comprehensive analysis of IM from an inter-temporal allocation perspective using non-progressive models, extending our previous work to incorporate agent heterogeneity. This approach offers a more realistic representation of influence dynamics in diverse populations, addressing a crucial factor often overlooked in previous studies. Second, we expand our investigation to include game-theoretical scenarios under uniform strategies, providing initial insights into competitive influence maximization in multi-agent environments. This novel aspect enhances our understanding of strategic interactions in settings where multiple entities compete for influence within the same network. Third, by employing the heterogeneous mean-field method and utilizing Taylor expansions, we derive analytical approximations that offer insights into the temporal dynamics of influence spread. These techniques enable us to quantify the timescales required for networks to reach equilibrium, with a particular focus on scale-free networks prevalent in many real-world systems. Our analytical framework significantly enhances the understanding of how influence propagates through complex network structures over time. Fourth, through extensive numerical experiments, we demonstrate the superiority of individually optimized influence strategies compared to uniform allocation approaches. This contribution highlights the importance of tailoring influence tactics to specific agents within a network, considering their unique characteristics and positions.

The key findings of our study reveal several important aspects of inter-temporal influence maximization. In the constant-opponent setting, we show that competing controllers can dominate the campaign at later stages by strategically timing their budget consumption. We also find that networks have a natural time scale for information propagation, requiring controllers to balance start-up time with the time needed for control to take effect. This implies different optimal starting times for networks with varying degrees of heterogeneity and different time horizons. In the game-theoretical setting, we demonstrate that the controller with a budget advantage should start earlier to ensure superiority in vote shares. Our analysis of individual optimization reveals that strategic allocation is most effective when resources are limited, focusing on low-degree nodes. Furthermore, we identify distinct regimes of optimal budget allocations and starting times in the presence of agents with different levels of zealotry.

Several promising directions for future work emerge from our study. First, while the voter model provides a solid analytical foundation for understanding inter-temporal influence strategies, it focuses on binary opinions and simple contagion, which simplify complex real-world opinion dynamics. Extending this framework to incorporate more sophisticated mechanisms, such as complex contagion or multi-state opinion formation models, presents an exciting opportunity to deepen our understanding of inter-temporal influence propagation in diverse social contexts. Additionally, our framework assumes complete knowledge of network topology, which offers clarity and precision in strategy optimization. However, in many real-world applications, such comprehensive information may be unavailable or impractical. Investigating scenarios with incomplete or probabilistic knowledge of network structure and opponent

strategies represents an important and challenging direction for future work. Exploring methods to optimize influence strategies under partial network visibility or uncertain opponent behaviors could also enhance the practical applicability of the framework.

A. Fully Flexible Resource Allocation in a One-Node System

In this section, we analyze optimal inter-temporal influence allocation for a single-node system (N = 1) involving two controllers, A and B. Both controllers have finite resource budgets over the time horizon T, given by $b_A =$ We focus on a constant-opponent scenario where controller A optimizes its influence allocation a(t) against a passive opponent *B*, whose influence $b(t) = \frac{b_B}{T}$ remains constant throughout the time horizon. The dynamics of the node's opinion, following Eq. (1), are described as:

$$\dot{x}(t) = \frac{a(t)}{a(t) + b(t)} - x(t),\tag{20}$$

where x(t) is the probability that the node holds opinion A at time t. The objective of controller A is to maximize its vote share at the final time T, given by:

$$S_A(T) = x(T). (21)$$

Assuming that controller A begins its influence at time t_0 , we set a(t) = 0 for $t < t_0$ and $a(t) = \hat{a}(t) \ge 0$ for $t \ge t_0$, and the initial condition for the opinion is $x(0) = x_0$. Solving the non-autonomous inhomogeneous differential equation of Eq. (20) yields:

$$x(T) = x_0 e^{-T} + e^{-T} \int_{t_0}^{T} e^t \frac{\hat{a}(t)}{\hat{a}(t) + b(t)} dt.$$
 (22)

The term $x_0 e^{-T}$ is constant, so maximizing x(T) reduces to maximizing the second term:

$$\int_{t_0}^T e^t \frac{\hat{a}(t)}{\hat{a}(t) + b(t)} dt,$$
(23)

subject to the budget constraint:

$$\int_{t_0}^{T} \hat{a}(t) dt = b_A, \quad \hat{a}(t) \ge 0 \text{ for } t \ge t_0.$$
 (24)

To solve this optimization problem, we use the calculus of variations. Introducing a Lagrange multiplier λ for the budget constraint, the functional to be maximized becomes:

$$\mathcal{L}(\hat{a},t) = \frac{\hat{a}(t)}{\hat{a}(t) + b(t)} e^t + \lambda \hat{a}(t). \tag{25}$$

Taking the derivative of \mathcal{L} with respect to $\hat{a}(t)$, we obtain:

$$\frac{b(t)e^t}{(\hat{a}(t) + b(t))^2} + \lambda = 0.$$
 (26)

Rearranging terms of Eq. (26) gives:

$$\hat{a}(t) = \sqrt{-\frac{b(t)}{\lambda}e^t} - b(t). \tag{27}$$

Substituting this into the budget constraint:

$$\int_{t_0}^T \hat{a}(t) dt = b_A, \tag{28}$$

allows us to eliminate λ , yielding the optimal control:

$$\hat{a}(t) = \frac{b_A + b(T - t_0)}{2\left(e^{T/2} - e^{t_0/2}\right)} e^{t/2} - b.$$
(29)

Additionally, the positivity condition $\hat{a}(t) \ge 0$ determines the starting time t_0 , where $\hat{a}(t_0) = 0$. Regarding this, the starting time t_0 is determined by solving the transcendental equation:

$$e^{(T-t_0)/2} - \frac{T-t_0}{2} = \frac{b_A}{2b} + 1. {30}$$

Here, the left-hand side $e^{(T-t_0)/2} - \frac{T-t_0}{2}$ depends on $T-t_0$, which determines how far from T the influence starts. On the other hand, the right-hand side grows with the ratio $\frac{b_A}{b}$. For larger $\frac{b_A}{b}$, the right-hand side becomes larger, so $T-t_0$ must increase to satisfy the equation. In other word, a larger budget for controller A relative to controller B allows A to start influencing earlier, which aligns with the conclusion drawn in Section 4.3.1.

B. Heterogeneous Mean-Field Analysis

Here we provide the detailed derivation of the heterogeneous mean-field analysis for vote share trajectories under temporal control. Starting from Eq. (1), we employ the heterogeneous mean-field approximation by grouping nodes of the same degree k. Under this framework, we approximate the neighbor influence term as:

$$\sum_{j} w_{ji} x_{j} \approx k_{i} \langle x \rangle, \tag{31}$$

where $k_i = \sum_j w_{ji}$ is the sum of incoming links of node *i* and $\langle x \rangle$ represents the average behaviour of a neighbour. Specifically, $\langle x \rangle$ is equal to

$$\langle x \rangle = \sum_{k} \frac{k}{\langle k \rangle} p_k x_k, \tag{32}$$

where p_k is the fraction of nodes with degree k and $\langle k \rangle = \sum_k k p_k$ is the average degree of the network. Note that $\frac{k}{\langle k \rangle}$ term stands for nodes with higher degree are more likely to be connected. Inserting Eq. (31) into Eq. (1) and rewriting for the dynamics of nodes with degree k, we have

$$\dot{x}_k = \frac{a_k}{k + a_k + b_k} + \frac{k \langle x \rangle}{k + a_k + b_k} - x_k,\tag{33}$$

where a_k and b_k stand for allocations to nodes with degree k. Multiplying Eq. (33) by $kp_k/\langle k \rangle$ and summing over k, we obtain a differential equation for $\langle x \rangle$

$$\frac{d}{dt}\langle x \rangle = \beta + \alpha \langle x \rangle \tag{34}$$

with coefficients

$$\alpha = \sum_{k} \frac{k^2 p_k}{\langle k \rangle} \frac{1}{k + a_k + b_k} - 1,$$

$$\beta = \sum_{k} \frac{k p_k a_k}{\langle k \rangle} \frac{1}{k + a_k + b_k},$$
(35)

which are constants for a given network. As Eq. (34) is a first-order differential equation, that can be solved by eigenvalue decomposition. Based on the assumption that controller B starts control at time 0 and controller A has the freedom to choose the starting time t_a , we calculate the probability that nodes with degree k will adopt A at time t ($t > t_a$) and the corresponding vote share as follows:

$$x_k(t) = \frac{a_k \alpha - \beta k + \frac{k e^{\alpha t} \left(\beta + \alpha x_k(t_a)\right)}{\alpha (a_k + b_k + k)}}{\alpha (a_k + b_k + k)} - e^{-t} \left(\frac{a_k \alpha - \beta k + \frac{k \left(\beta + \alpha x_k(t_a)\right)}{\alpha + 1}}{\alpha (a_k + b_k + k)} - x_k(t_a) \right), \tag{36}$$

$$S_A(t) = \sum_k p_k x_k(t),$$

Competitive Influence Maximization in Voter Dynamics: The Role of Timing and Network Heterogeneity

where

$$\gamma = \sum_{k} \frac{k^{2} p_{k}}{\langle k \rangle} \frac{1}{k + b_{k}} - 1,$$

$$x_{k}(t_{a}) = x_{0} e^{-t_{a}} + \frac{k}{k + b_{k}} x_{0} \left(e^{\gamma t_{a}} (1 - e^{-t_{a}}) \right).$$
(37)

Here, $x_k(t_a)$ is the probability of nodes of degree k holding opinion A at time t_a .

C. Synthetic Network Generation

To investigate the impact of network heterogeneity on influence propagation under temporal control, we generate synthetic networks using the configuration model [15]. This model enables the creation of networks with precisely controlled degree distributions, allowing us to replicate the scale-free structures commonly observed in real-world networks. Moreover, it allows systematic exploration of how variations in power-law degree distributions influence network dynamics while maintaining other network properties, such as the average degree $\langle k \rangle$, approximately constant.

The network generation process consists of two main steps. First, each vertex i in a network of size N is assigned a degree k_i drawn from a power-law degree distribution, defined as:

$$p_k = ck^{-\lambda}, \quad k_{\min} \le k \le k_{\max}, \tag{38}$$

where c is the normalization coefficient, k_{\min} is the minimum degree, and k_{\max} is the maximum degree that serves as a structural cut-off to prevent degree correlations from finite-size effects [7]. Moreover, the parameter λ determines the network's degree heterogeneity, with smaller values producing networks with highly connected hubs and larger values yielding more homogeneous structures. Second, node stubs (half-edges) are randomly paired to form edges. To ensure network validity, we rewire stubs to remove self-loops and multi-edges while preserving the target degree distribution as closely as possible.

To enable fair comparisons across networks with different λ , we keep the average degree $\langle k \rangle$ approximately constant by adjusting k_{\min} according to the following constraints:

$$\sum_{k=k_{\min}}^{k_{\max}} ck^{-\lambda} = 1,$$

$$\sum_{k=k_{\min}}^{k_{\max}} ck^{-\lambda+1} = \langle k \rangle,$$
(39)

which establishes a direct relationship between network parameters. Here, the first equation ensures the sum of the probabilities for all possible degrees must equal 1, while the second equation ensures that the average degree matches the desired target. By numerically solving these equations, we can determine k_{\min} for each λ , given the target $\langle k \rangle$ and k_{\max} . Note that, since k_{\min} must be an integer, slight deviations in $\langle k \rangle$ can occur. For example, a target $\langle k \rangle = 10$ yields an actual $\langle k \rangle = 10.5$, as shown in Figs. 2, 4 and 8.

Specifically, for larger networks (i.e., $N=10^4$), we set $k_{\rm max}=\sqrt{N}$, following the natural cutoff scaling observed in uncorrelated networks [15], and specify a target average degree $\langle k \rangle = 10$. Note that, while our synthetic dataset focuses on isolating the influence of network heterogeneity by fixing target average degree as 10, we also validate our findings using real-world networks with varying average degrees (see Tables 1 and 2). For computationally demanding individual optimization experiments (Figs. 6 and 7), we use smaller networks with $N=10^2$ nodes. In these cases, we set $k_{\rm max}=30$ and $\langle k \rangle=6$, which balances a sufficiently broad degree range with the need to avoid excessive degree correlations. Additionally, to systematically explore the effects of degree heterogeneity, we vary the power-law exponent λ from 1.6 to 5. This range captures both highly heterogeneous networks (low λ) and more homogeneous ones (high λ). The lower bound $\lambda=1.6$ is chosen because values below this threshold fail to yield a discrete $k_{\rm min}$ that satisfies the constraints defined in Eq. (39), and aligns with real-world networks where heterogeneity typically around or exceeds 1.6 [16, 29].

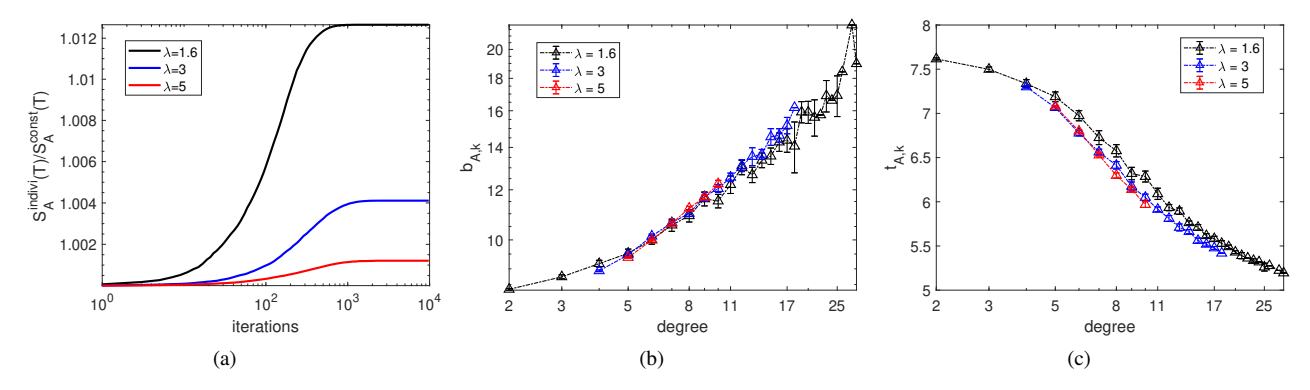


Figure 10: Fig. (a) shows the optimization process characterized by the dependence of average relative vote share $S_A^{indivi}(T)/S_A^{const}(T)$ on iterations of the optimization algorithm. $S_A^{indivi}(T)$ stands for vote shares at time T calculated by individual optimization while $S_A^{const}(T)$ represents vote shares calculated by assigning a single optimized starting time for the whole network. The black line, blue line, and red line stand for networks with degree of heterogeneity $\lambda=1.6$, $\lambda=3$ and $\lambda=5$ respectively. Figs. (b) and (c) show the corresponding distributions of budget allocations and starting times on nodes with degree k when the system depicted in Fig. (a) reaches the maximum in the scenario of individual optimization. All the calculations are based on networks with $N=10^2$ and $\langle k \rangle=6$ and tested in 10 realizations. The control gains of controller B pertaining to each node are all fixed as 1 per unit time from time 0. The time horizon T is set as T=10. The total budgets of controller A are set to be the same as controller B's, i.e., $b_A=b_B=N\times T$. The initial states of opinion distribution are 0 for all nodes. Error bars indicate 95% confidence intervals.

D. Individual Optimization for the Special Case of $b_A = b_B$

In Fig. 10 (a), we evaluate the performance of individual optimization by showing the vote shares achieved by optimization with node-specific starting times and budget allocations relative to the simple scenario where the optimized controller assigns a single starting time for the whole network. From our analysis of Fig. 10 (a), we observe that, roughly N^2 iterations yield near-optimal allocations, as each node is updated N times on average and no further improvements are observed beyond this point. Therefore, in the individual optimization experiments, we set $L_{max} = N^2$.

Even though the improvements of vote shares achieved by individual optimization are very small, a clear difference in vote shares achievable for networks with different degrees of heterogeneity is apparent. Specifically, individual optimization is relatively more efficient for networks with larger heterogeneity. A possible explanation for this observation is that the degrees of highly heterogeneous networks are distributed over a larger range compared with less heterogeneous networks and thus differences between degrees can be fully exploited in the individual optimization case. To further confirm our hypothesis, in Figs. 10 (b) and (c), we present the dependence of optimized budget allocations $(b_{A,k})$ and starting times $(t_{A,k})$ on the degree. Two observations stand out. First, we note a positive correlation between budget allocations and degrees (see panel (b)). Second, it is apparent that there is an inverse relationship between nodes' degrees and starting times. This implies that a node with a larger degree should be allocated more resources and the campaign for such a node should start earlier. Moreover, we also find that networks with different degrees of heterogeneity have a similar distribution of budget allocations and starting times regarding nodes' degrees.

E. Individual Optimization Considering Agent Heterogeneity in Complete Networks

To gain some intuition about how different levels of zealotry influence optimal starting times and budget allocations, we also explore influence-maximizing strategies in a complete network with a uniform distribution of zealotry in the range [0, 1]. Here, the complete network is chosen for its simplicity, which allows us to focus on the effects of zealotry without the added complexity of network structure. Moreover, we use the above-mentioned stochastic hill climbing algorithm to determine both the optimized control gains and starting times in the presence of zealotry.

From Figs. 11 (a) and (b), we identify two regimes of optimal control gains and starting times. For small budget ratios (e.g., $b_A/b_B = 0.1$, 1), controller A only targets nodes with low to moderate levels of zealotry. In these scenarios, control gains decrease as zealotry increases, and the optimal starting times shift to later periods. In contrast, when the

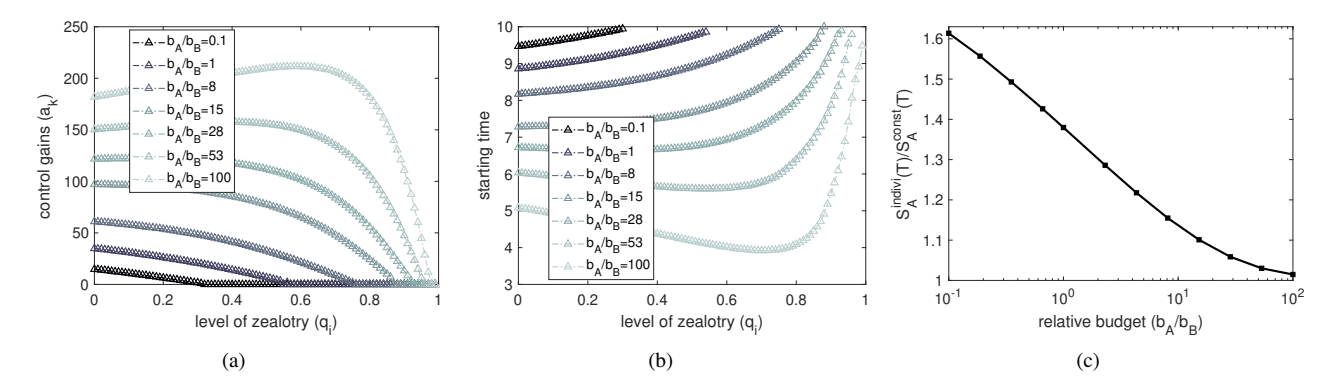


Figure 11: Figs. (a) and (b) show the dependence of control gains and starting times on the level of zealotry q_i and relative budget b_A/b_B obtained via the individual optimization method on a complete network with size $N=10^2$. Fig. (c) shows the resulting improvements of vote shares via individual optimization compared with assigning a single optimized starting time for the whole network for varying relative budgets. The control gains of controller B pertaining to each node are all fixed as 1 per unit time from time B. The time horizon B is set as B in the initial states of opinion distribution are B for all nodes.

budget ratio is large (e.g., $b_A/b_B = 100$), controller A adjusts its strategy based on the level of zealotry. Before reaching a critical level of zealotry (around $q_i \approx 0.7$), controller A allocates more resources and starts the influence campaign earlier as zealotry increases. However, beyond this threshold level of zealotry, the pattern reverses: as zealotry continues to increase, controller A begins to allocate fewer resources and delays the starting times. This reversal can be attributed to the diminishing returns of influence efforts on highly zealous nodes, who are already inclined towards the desired opinion. Therefore, investing additional resources in these nodes becomes less effective. Additionally, Fig. 11 (c) supports the findings from Fig. 6 (a), that individual optimization is more effective with smaller budgets, as it allows the controller to focus on a select few nodes.

Acknowledgement

The authors acknowledge the use of the IRIDIS High Performance Computing Facility in the completion of this work. ZC acknowledges support from the High-level Talent Project of Xiamen University of Technology (YKJ24021R). MB acknowledges support from the Alan Turing Institute (EPSRC grant EP/N510129/1, https://www.turing.ac.uk/) and the Royal Society (grant IES\R2\192206, https://royalsociety.org/).

References

- [1] Ali, K., Wang, C.Y., Chen, Y.S., 2019. A novel nested q-learning method to tackle time-constrained competitive influence maximization. IEEE Access 7, 6337–6352. doi:10.1109/ACCESS.2018.2888895.
- [2] Ali, K., Wang, C.Y., Chen, Y.S., 2022. Leveraging transfer learning in reinforcement learning to tackle competitive influence maximization. Knowledge and Information Systems 64, 2059–2090. doi:10.1007/s10115-022-01696-3.
- [3] Alshamsi, A., Pinheiro, F.L., Hidalgo, C.A., 2017. When to target hubs? Strategic diffusion in complex networks. arXiv CoRR abs/1705.00232. URL: http://arxiv.org/abs/1705.00232, arXiv:1705.00232.
- [4] Anstreicher, K.M., 2009. Linear programming: Interior point methods, in: Floudas, C.A., Pardalos, P.M. (Eds.), Encyclopedia of Optimization, Second Edition. Springer, pp. 1886–1889. doi:10.1007/978-0-387-74759-0_337.
- [5] Badawy, A., Ferrara, E., Lerman, K., 2018. Analyzing the digital traces of political manipulation: The 2016 russian interference twitter campaign, in: Brandes, U., Reddy, C., Tagarelli, A. (Eds.), IEEE/ACM 2018 International Conference on Advances in Social Networks Analysis and Mining, ASONAM 2018, Barcelona, Spain, August 28-31, 2018, IEEE Computer Society. pp. 258-265. URL: https://doi.org/10.1109/ASONAM.2018.8508646, doi:10.1109/ASONAM.2018.8508646.
- [6] Bharathi, S., Kempe, D., Salek, M., 2007. Competitive influence maximization in social networks, in: Deng, X., Graham, F.C. (Eds.), Internet and Network Economics, Third International Workshop, WINE 2007, San Diego, CA, USA, December 12-14, 2007, Proceedings, Springer. pp. 306–311. URL: https://doi.org/10.1007/978-3-540-77105-0_31, doi:10.1007/978-3-540-77105-0_31.
- [7] Boguná, M., Pastor-Satorras, R., Vespignani, A., 2004. Cut-offs and finite size effects in scale-free networks. The European Physical Journal B 38, 205–209.

- [8] Bonomi, G., Gatti, N., Panozzo, F., Restelli, M., 2012. Computing equilibria with two-player zero-sum continuous stochastic games with switching controller, in: Hoffmann, J., Selman, B. (Eds.), Proceedings of the Twenty-Sixth AAAI Conference on Artificial Intelligence, July 22-26, 2012, Toronto, Ontario, Canada, AAAI Press. pp. 1270–1277. URL: https://doi.org/10.1609/aaai.v26i1.8238, doi:10.1609/AAAI.V26I1.8238.
- [9] Braha, D., De Aguiar, M.A., 2017. Voting contagion: Modeling and analysis of a century of us presidential elections. PloS one 12, e0177970.
- [10] Brede, M., Restocchi, V., Stein, S., 2019. Effects of time horizons on influence maximization in the voter dynamics. Journal of Complex Networks 7, 445–468. URL: https://doi.org/10.1093/comnet/cny027, doi:10.1093/comnet/cny027.
- [11] Budak, C., Agrawal, D., Abbadi, A.E., 2011. Limiting the spread of misinformation in social networks, in: Srinivasan, S., Ramamritham, K., Kumar, A., Ravindra, M.P., Bertino, E., Kumar, R. (Eds.), Proceedings of the 20th International Conference on World Wide Web, WWW 2011, Hyderabad, India, March 28 April 1, 2011, ACM. pp. 665–674. URL: https://doi.org/10.1145/1963405.1963499, doi:10.1145/1963405.1963499.
- [12] Cai, Z., Brede, M., Gerding, E.H., 2020. Influence maximization for dynamic allocation in voter dynamics, in: Benito, R.M., Cherifi, C., Cherifi, H., Moro, E., Rocha, L.M., Sales-Pardo, M. (Eds.), Complex Networks & Their Applications IX Volume 1, Proceedings of the Ninth International Conference on Complex Networks and Their Applications, COMPLEX NETWORKS 2020, 1-3 December 2020, Madrid, Spain, Springer. pp. 382–394. URL: https://doi.org/10.1007/978-3-030-65347-7_32, doi:10.1007/978-3-030-65347-7_32.
- [13] Carnes, T., Nagarajan, C., Wild, S.M., van Zuylen, A., 2007. Maximizing influence in a competitive social network: A follower's perspective, in: Proceedings of the 9th International Conference on Electronic Commerce: The Wireless World of Electronic Commerce, 2007, University of Minnesota, Minneapolis, MN, USA, August 19-22, 2007, ACM. pp. 351–360. doi:10.1145/1282100.1282167.
- [14] Castellano, C., Fortunato, S., Loreto, V., 2009. Statistical physics of social dynamics. Review of Modern Physics 81, 591-646. URL: https://link.aps.org/doi/10.1103/RevModPhys.81.591, doi:10.1103/RevModPhys.81.591.
- [15] Catanzaro, M., Boguná, M., Pastor-Satorras, R., 2005. Generation of uncorrelated random scale-free networks. Physical Review E 71, 1–4. doi:10.1103/PhysRevE.71.027103.
- [16] Clauset, A., Shalizi, C.R., Newman, M.E., 2009. Power-law distributions in empirical data. SIAM review 51, 661–703.
- [17] Curran, P., 2009. On a variation of the gershgorin circle theorem with applications to stability theory, in: Irish Signals and Systems Conference (ISSC 2009), IET. p. 1–5. doi:10.1049/cp.2009.1687.
- [18] Dawood, Y., 2021. Combatting foreign election interference: Canada's electoral ecosystem approach to disinformation and cyber threats. Election Law Journal: Rules, Politics, and Policy 20, 10–31. doi:10.1089/elj.2020.0652.
- [19] Fernández-Gracia, J., Suchecki, K., Ramasco, J.J., San Miguel, M., Eguíluz, V.M., 2014. Is the Voter Model a Model for Voters? Physical Review Letters 112, 1-15. URL: https://link.aps.org/doi/10.1103/PhysRevLett.112.158701, doi:10.1103/PhysRevLett. 112.158701.
- [20] Ferreira, M., Andrade, M., Matos, M.C.P., Filipe, J., Coelho, M., 2012. Minimax theorem and Nash equilibrium. The International Journal of Latest Trends in Finance and Economic Sciences 2, 36–40.
- [21] Fire, M., Puzis, R., 2016. Organization mining using online social networks. Networks and Spatial Economics 16, 545-578.
- [22] Galam, S., Javarone, M.A., 2016. Modeling radicalization phenomena in heterogeneous populations. PLOS ONE 11, 1–15. doi:10.1371/journal.pone.0155407.
- [23] Goyal, A., Bonchi, F., Lakshmanan, L.V.S., Venkatasubramanian, S., 2013. On minimizing budget and time in influence propagation over social networks. Social Network Analysis and Mining 3, 179–192. doi:10.1007/s13278-012-0062-z.
- [24] Goyal, S., Heidari, H., Kearns, M., 2019. Competitive contagion in networks. Games and Economic Behavior 113, 58–79. doi:10.1016/j.geb.2014.09.002.
- [25] Guo, S., Xu, H., Zhang, L., 2021. Existence and approximation of continuous bayesian nash equilibria in games with continuous type and action spaces. SIAM Journal on Optimization 31, 2481–2507.
- [26] Hegselmann, R., König, S., Kurz, S., Niemann, C., Rambau, J., 2015. Optimal opinion control: The campaign problem. Journal of Artificial Societies & Social Simulation 18, 1–12.
- [27] Huang, F., Chen, H.S., 2019. An improved heterogeneous mean-field theory for the Ising model on complex networks. Communications in Theoretical Physics 71, 1475–1479. doi:10.1088/0253-6102/71/12/1475.
- [28] Kempe, D., Kleinberg, J.M., Tardos, É., 2003. Maximizing the spread of influence through a social network, in: Getoor, L., Senator, T.E., Domingos, P.M., Faloutsos, C. (Eds.), Proceedings of the Ninth ACM SIGKDD International Conference on Knowledge Discovery and Data Mining, Washington, DC, USA, August 24 27, 2003, ACM. pp. 137–146. URL: https://doi.org/10.1145/956750.956769, doi:10.1145/956750.956769.
- [29] Kunegis, J., 2013. Konect: the koblenz network collection, in: Proceedings of the 22nd international conference on world wide web, pp. 1343–1350.
- [30] Lambiotte, R., Saramäki, J., Blondel, V.D., 2009. Dynamics of latent voters. Physical Review E—Statistical, Nonlinear, and Soft Matter Physics 79, 046107.
- [31] Leskovec, J., Huttenlocher, D., Kleinberg, J., 2010. Governance in social media: A case study of the wikipedia promotion process, in: Proceedings of the International AAAI Conference on Web and Social Media, pp. 98–105.
- [32] Leskovec, J., Mcauley, J., 2012. Learning to discover social circles in ego networks. Advances in neural information processing systems 25.
- [33] Li, Y., Gao, H., Gao, Y., Guo, J., Wu, W., 2023. A survey on influence maximization: From an ml-based combinatorial optimization. ACM Transactions on Knowledge Discovery from Data 17, 133:1–133:50. URL: https://doi.org/10.1145/3604559, doi:10.1145/3604559.
- [34] Liu, B., Cong, G., Xu, D., Zeng, Y., 2012. Time constrained influence maximization in social networks, in: 12th IEEE International Conference on Data Mining, ICDM 2012, Brussels, Belgium, December 10-13, 2012, IEEE Computer Society. pp. 439–448. doi:10.1109/ICDM.2012. 158.
- [35] Liu, S., Ying, L., Shakkottai, S., 2010. Influence maximization in social networks: An Ising-model-based approach, in: 48th Annual Allerton Conference on Communication, Control, and Computing, Allerton 2010, Monticello, IL, USA, September 29 - October 1, 2020, IEEE. pp.

- 570-576. URL: https://doi.org/10.1109/ALLERTON.2010.5706958, doi:10.1109/ALLERTON.2010.5706958.
- [36] Loizou, N., Vaswani, S., Laradji, I.H., Lacoste-Julien, S., 2021. Stochastic polyak step-size for SGD: an adaptive learning rate for fast convergence, in: Banerjee, A., Fukumizu, K. (Eds.), The 24th International Conference on Artificial Intelligence and Statistics, AISTATS 2021, April 13-15, 2021, Virtual Event, PMLR. pp. 1306–1314. URL: http://proceedings.mlr.press/v130/loizou21a.html.
- [37] Lu, H., 2007. On the existence of pure-strategy nash equilibrium. Economics Letters 94, 459–462.
- [38] Massa, P., Salvetti, M., Tomasoni, D., 2009. Bowling alone and trust decline in social network sites, in: 2009 Eighth IEEE International Conference on Dependable, Autonomic and Secure Computing, IEEE. pp. 658–663.
- [39] Masuda, N., 2015. Opinion control in complex networks. New Journal of Physics 17, 1–12. doi:10.1088/1367-2630/17/3/033031.
- [40] Masuda, N., Gibert, N., Redner, S., 2010. Heterogeneous voter models. Physical Review E 82, 1-4. doi:10.1103/PhysRevE.82.010103.
- [41] Moreno, G.R., Manino, E., Tran-Thanh, L., Brede, M., 2020. Zealotry and influence maximization in the voter model: When to target partial zealots?, in: Barbosa, H., Gomez-Gardenes, J., Gonçalves, B., Mangioni, G., Menezes, R., Oliveira, M. (Eds.), Complex Networks XI. Springer International Publishing Switzerland. Springer Proceedings in Complexity, pp. 107–118. URL: https://complenetlive20.weebly.com/, doi:10.1007ConferenceonComplexNetworks:CompleNetLive2020, CompleNetLive2020;Conferencedate:19-08-2020Through20-08-2020.
- [42] Morone, F., Makse, H.A., 2015. Influence maximization in complex networks through optimal percolation. Nature 524, 65–68. doi:10.1038/nature14604
- [43] Newman, M.E., 2005. Power laws, pareto distributions and zipf's law. Contemporary physics 46, 323-351.
- [44] Palermo, G., Mancini, A., Desiderio, A., Di Clemente, R., Cimini, G., 2024. Spontaneous opinion swings in the voter model with latency. Physical Review E 110, 024313.
- [45] Pérez, T., Klemm, K., Eguíluz, V.M., 2016. Competition in the presence of aging: dominance, coexistence, and alternation between states. Scientific Reports 6, 21128.
- [46] Rajabi, A., Mantzaris, A.V., Atwal, K.S., Garibay, I., 2021. Exploring the disparity of influence between users in the discussion of Brexit on Twitter: Twitter influence disparity in Brexit. Journal of Computational Social Science 4, 903–917. URL: https://doi.org/10.1007/s42001-021-00112-0, doi:10.1007/S42001-021-00112-0.
- [47] Ramos, M., Shao, J., Reis, S.D., Anteneodo, C., Andrade, J.S., Havlin, S., Makse, H.A., 2015. How does public opinion become extreme? Scientific Reports 5, 1–14. doi:10.1038/srep10032.
- [48] Razali, G., Nikmah, M., Sutaguna, I.N.T., Putri, P.A.N., Yusuf, M., 2023. The influence of viral marketing and social media marketing on instagram adds purchase decisions. CEMERLANG: Jurnal Manajemen dan Ekonomi Bisnis 3, 75–86.
- [49] Redner, S., 2019. Reality-inspired voter models: A mini-review. Comptes Rendus Physique 20, 275-292. URL: https://www.sciencedirect.com/science/article/pii/S1631070519300325, doi:https://doi.org/10.1016/j.crhy.2019.05.004.
- [50] Singh, S.S., Srivastva, D., Verma, M., Singh, J., 2022. Influence maximization frameworks, performance, challenges and directions on social network: A theoretical study. Journal of King Saud University-Computer and Information Sciences 34, 7570–7603.
- [51] Son, S.W., Jeong, H., Hong, H., 2008. Relaxation of synchronization on complex networks. Physical Review E 78, 1–7. doi:10.1103/ PhysRevE.78.016106.
- [52] Thomas, M., Pang, B., Lee, L., 2006. Get out the vote: Determining support or opposition from congressional floor-debate transcripts. arXiv preprint cs/0607062.
- [53] Tong, G., Wang, R., Dong, Z., Li, X., 2021. Time-constrained adaptive influence maximization. IEEE Transactions on Computational Social Systems 8, 33–44. doi:10.1109/TCSS.2020.3032616.
- [54] Vendeville, A., Guedj, B., Zhou, S., 2021. Forecasting elections results via the voter model with stubborn nodes. Applied Network Science 6, 1–13.
- [55] Wilder, B., Vorobeychik, Y., 2018. Controlling elections through social influence, in: the 17th International Conference on Autonomous Agents and Multiagent Systems, International Foundation for Autonomous Agents and Multiagent Systems, Richland, SC. p. 265–273.